The Abdus Salam
International Centre for Theoretical Physics

United Nations
Educational, Scientific and
Cultural Organization

IAEA
International Atomic Energy Agency

1965-24

9th Workshop on Three-Dimensional Modelling of Seismic Waves Generation, Propagation and their Inversion

22 September - 4 October, 2008

Stress Fields and Fluids In Rock Masses

F.H. Cornet
Inst. Phys. du Globe de Strasbourg
Strasbourg
France

françois.cornet@eost.u-strasbg.fr

Stress Fields and Fluids In Rock Masses

F.H. Cornet; Inst. Phys. du Globe de Strasbourg (France);
françois.cornet@eost.u-strasbg.fr

Talk 1 : Basic concepts

1. Some elementary Rock Mechanics principles

2. Seismicity induced by fluid pressure variations

3. Regional stress field determination

Talk 2 : Examples of fluid induced seismicity

1. The Soultz/Forêts experimental geothermal site in the Rhine Graben (France)

2. The swarm activity in the Corinth Rift (Greece)

Some Elementary Rock Mechanics principles

- The stress vector and the Mohr circles
- Griffith's fracture criterion and Irwin's basic fracture modes
- The mechanics of hydraulic fracturing
- Stress failure criteria for rock masses in compression
  - Failure criteria for intact rocks
  - Failure along preexisting weakness planes
  - Failure development in the rock mass

Stress tensor and Stress vector

- For the surface S with unit area and normal **n** centered at **x,** the stress vector is defined as a function of the stress tensor σ and of the surface orientation **n** :

  $$\mathbf{t} = \sigma(\mathbf{x})\,\mathbf{n} \qquad (1)$$

- The stress vector has a normal component, (called the normal stress, it is a scalar)) :

  $$\sigma_n = \sigma(\mathbf{x})\,\mathbf{n} \cdot \mathbf{n} \qquad (2)$$

- and a shear component (vector):

  $$\tau = \sigma(\mathbf{x})\,\mathbf{n} - (\sigma(\mathbf{x})\,\mathbf{n} \cdot \mathbf{n})\,\mathbf{n} \qquad (3)$$

- The stress tensor has 6 components defined either in a general (geographical) frame of reference (σ_{ij}), or in the frame of reference of its eigen vectors (σ_i ; φ, ψ, θ = Euler angles that define the 3 eigen vectors orientation $\mathbf{e}_i$)

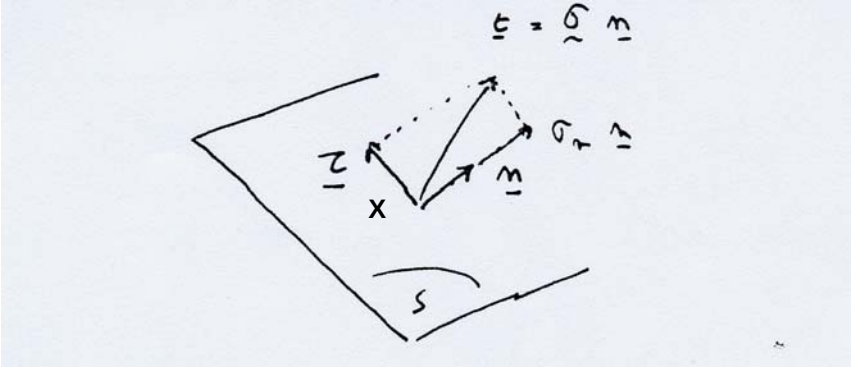

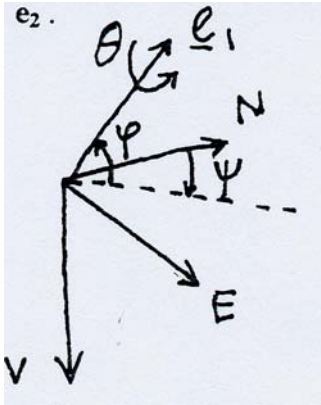

Mohr representation

- Given that σ_n and $|\tau|$ vary with the orientation of **n**, the set of all couples of values σ_n and $|\tau|$ corresponds to the area limited by the three Mohr circles

- When n is perpendicular to e_2 , the values for σ_n and $|\tau|$ are :

$$\sigma_n = (\sigma_1 + \sigma_3) / 2 + [(\sigma_1 - \sigma_3)/2] \cos (2\beta)$$

$$|\tau| = [(\sigma_1 - \sigma_3) / 2] \sin (2\beta)$$

Where β is angle of **n** w.r. to σ_1 direction

- In rock mechanics, the stress tensor is supposed to be uniform within an Elementary Representative Volume (ERV)

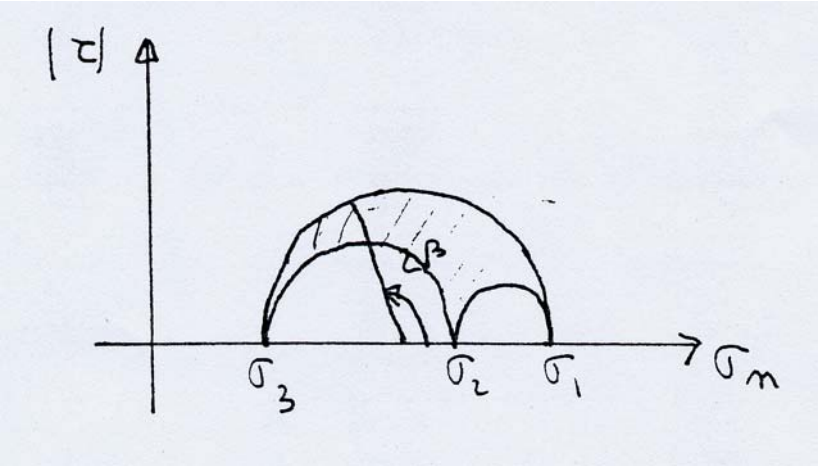

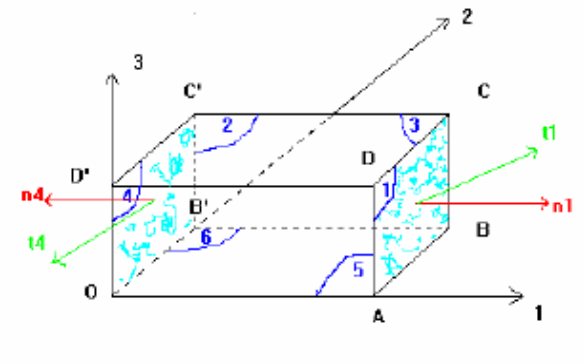

The role of microfissures on the local stress field (from Jaeger and Cook, 1976)

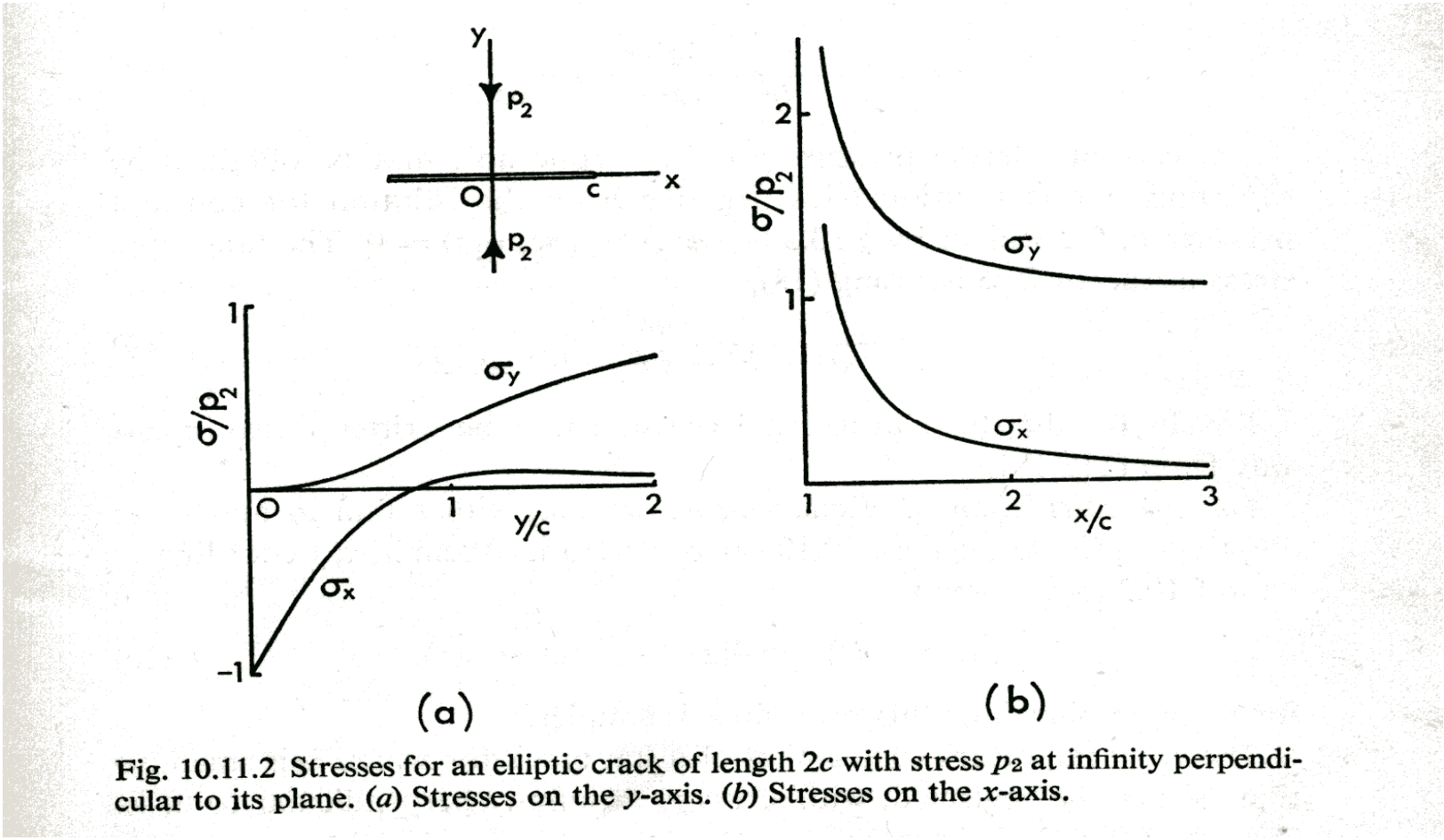

Fig. 10.11.2 Stresses for an elliptic crack of length $2c$ with stress p_2 at infinity perpendicular to its plane. (*a*) Stresses on the y-axis. (*b*) Stresses on the x-axis.

The Griffith energy criterion of failure

- ΔW (**ds**) = ΔU (**ds**) + ΔT (**ds**) + ΔD (**ds**)
  - Crack increment **ds** = **n**da
  - ΔW (**ds**) : work of external forces
  - ΔU (**ds**) : Elastic strain energy variation
  - ΔT (**ds**) : variation in kinetic energy
  - ΔD (**ds**) : variation in surface energy = γ da, with γ surface energy per unit area

- Strain Energy Release Rate : G = lim (ΔW (**ds**) - ΔU (**ds**)) / da when da $\rightarrow$ 0
- In adiabatic processes, there is rupture when G = 2 γ

  If dG / da < 0 ; fracture growth is stable; if dG / da > 0 ; fracture growth is unstable

- Kaiser effect : seismic signal generated by stable fracturing process; if the load is maintained constant activity stops. When load is increased, the fracturing starts again but does not lead to large scale instability

Irwin’s basic modes of fracture

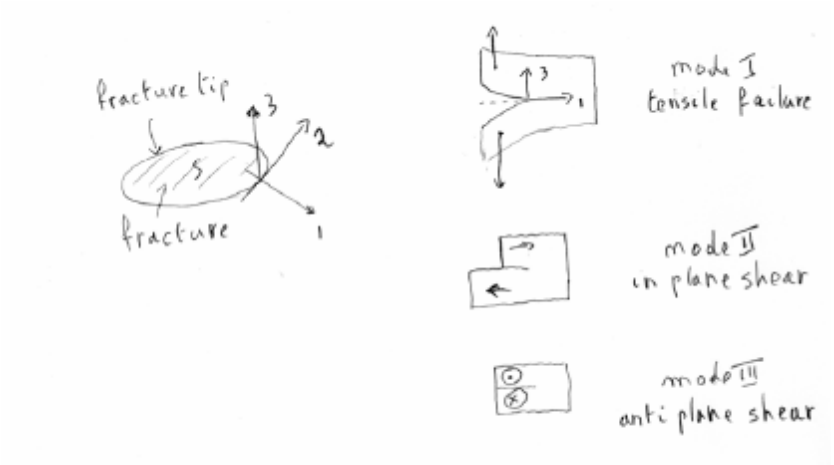

- Because the elastic strain energy variation is entirely dependent on the stress singularity close to the fracture tip, it suffices to investigate values of G close to the fracture tip . Three basic mode of fracture are defined
- Each basic mode is characterized by the stress intensity factor that characterizes the stress singularity near the fracture tip. It is an elastic problem (K_I, K_{II}, K_{III}).
- The stress intensity factors help compute the elastic strain energy released by fracture propagation, a quantity that is equated with the surface energy through the critical strain energy release rate.

Hydraulic fracturing

- The stress field close to a cylindrical hole in an elastic field is :

$$\sigma_{\rho\rho} = \left(1-\frac{r^2}{\rho^2}\right)\frac{\sigma_{11}^{\infty}+\sigma_{22}^{\infty}}{2} + \left(1-\frac{4r^2}{\rho^2}+\frac{3r^4}{\rho^4}\right)\left[\frac{\sigma_{11}^{\infty}-\sigma_{22}^{\infty}}{2}\cos 2\theta + \sigma_{12}^{\infty}\sin 2\theta\right]$$

$$\sigma_{\theta\theta} = \left(1+\frac{r^2}{\rho^2}\right)\frac{\sigma_{11}^{\infty}+\sigma_{22}^{\infty}}{2} - \left(1+\frac{3r^2}{\rho^2}\right)\left[\frac{\sigma_{11}^{\infty}-\sigma_{22}^{\infty}}{2}\cos 2\theta + \sigma_{12}^{\infty}\sin 2\theta\right]$$

$$\sigma_{zz} = \sigma_{33}^{\infty} - 4\nu\frac{r^2}{\rho^2}\left[\frac{\sigma_{11}^{\infty}-\sigma_{22}^{\infty}}{2}\cos 2\theta + \sigma_{12}^{\infty}\sin 2\theta\right]$$

$$\sigma_{\theta z} = \left(1+\frac{r^2}{\rho^2}\right)(\sigma_{23}^{\infty}\cos\theta - \sigma_{31}^{\infty}\sin\theta)\ ;\ \sigma_{z\rho} = \left(1-\frac{r^2}{\rho^2}\right)(\sigma_{31}^{\infty}\cos\theta + \sigma_{23}^{\infty}\sin\theta)$$

$$\sigma_{\theta\rho} = \left(1+\frac{2r^2}{\rho^2}-\frac{3r^4}{\rho^4}\right)\left[\frac{\sigma_{22}^{\infty}-\sigma_{11}^{\infty}}{2}\sin 2\theta + \sigma_{12}^{\infty}\cos 2\theta\right]$$

- If the borehole is parallel to a principal stress direction (Vertical) and a pressure is applied in the hole: $\sigma_{\theta\theta} = (\sigma_H + \sigma_h) - 2(\sigma_H - \sigma_h)\cos 2\theta - P_w$, and rupture occurs for :

$$\sigma_{\theta\theta} = -\sigma_H + 3\sigma_h - P_w + \sigma^T$$

- If the rock has been cooled down by mud circulation, the hoop stress is : $\sigma_{\theta\theta} = -K\Delta T / E$, where K is coefficient of thermal expansion, E is Young's modulus and ΔT is the difference between far-field and borehole temperature

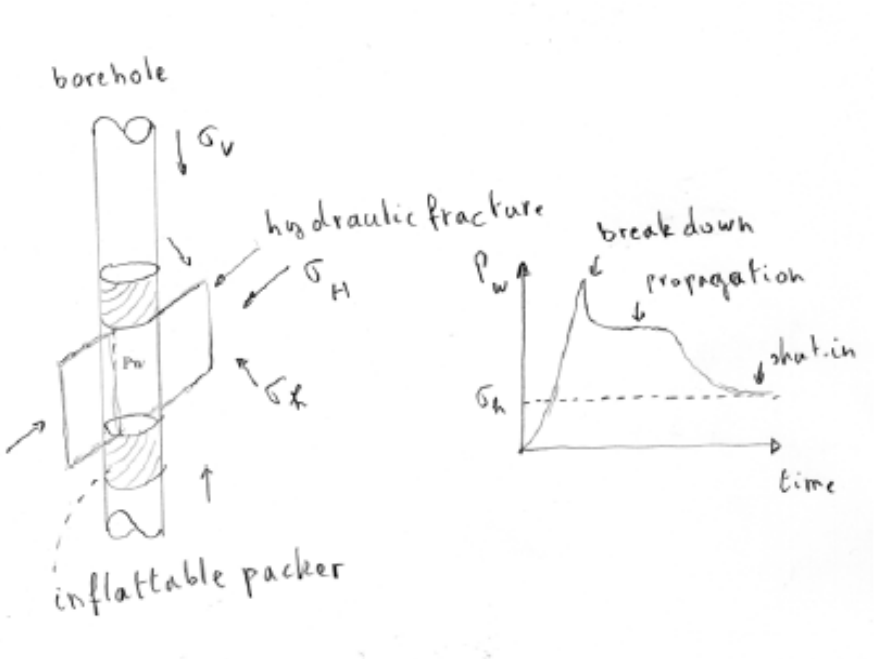

- Both hydraulic fracturing and thermal cracking are mode I fractures

Stress criteria for failure in compression

- Intact rocks
  - Tresca criterion

$$(\sigma_1 - \sigma_3) = K$$

  - Coulomb criterion (fracture orientation depends on stress field)

  - M
  - E nciple

$$|\tau| = \mu \sigma_n + C_0$$

- Failure along pre-existing weakness planes $\sigma' = \sigma - P\mathbf{I}$
  - Coulomb's friction law (failure plane is imposed) :

  - Byerlee's law

$$|\tau| = \mu (\sigma_n - P) + C_0$$

$$|\tau| = \mu (\sigma_n - P);\ 0.6 \leq \mu \leq 0.8$$

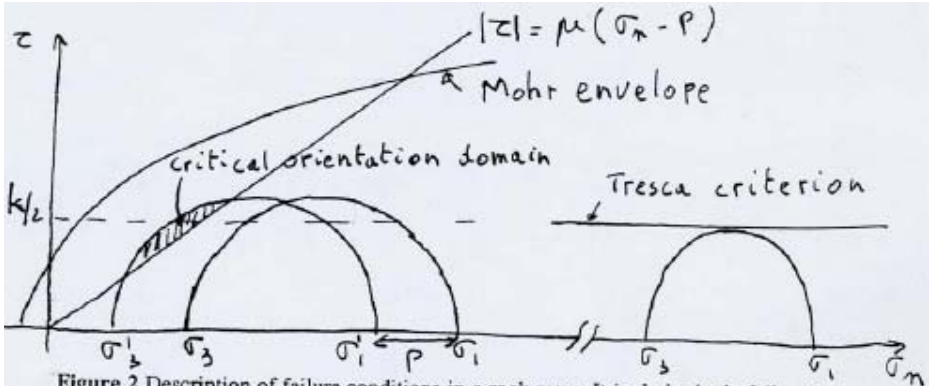

Figure 2 Description of failure conditions in a rock mass. It includes both, failure in the intact rock and failure along preexisting weakness planes as expressed in terms of effective stresses.

- Seismicity occurring in the upper 15 to 20 km of the crust involves fracture planes that make an unknown angle with respect to the principal stress directions.

- Shear displacement along preexisting fractures (faults ?) results in dilatancy and then contractancy

Acoustic emission during triaxial testing and the Kaiser effect

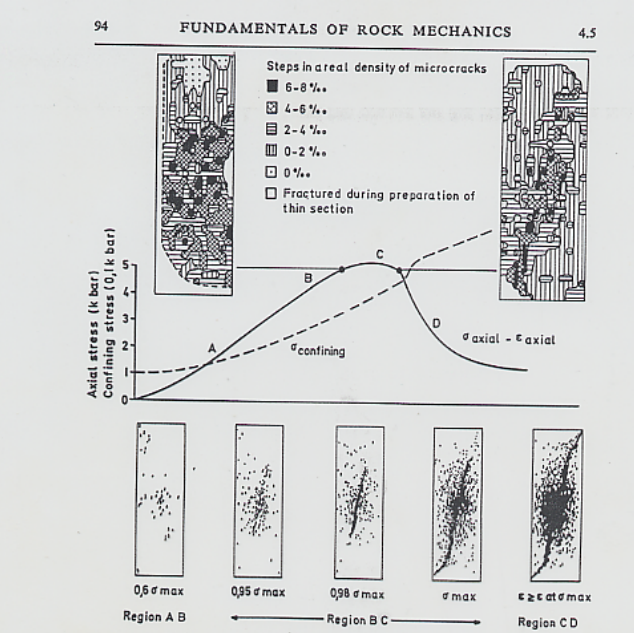

Fig. 4.5.2 A composite representation of the complete stress–strain curve and the incremental radial stress–axial strain curve for a suite of triaxial compression tests done in a stiff-testing machine and in a stiff, sealed triaxial cell, using specimens of argillaceous quartzite prepared from a single piece of rock. The axial sections through specimens stopped at various stages of compression show the structural changes associated with the complete stress–strain curve and associated dilatancy (after Hallbauer *et al.*, 1973).

The appearance of fracture surfaces has been little studied despite the importance of correlating laboratory effects with those observed in the field. Slickensides are commonly produced in shear fracture, and Paterson (1958) showed that for marble the direction of motion was that for which the steps would approach one another. When fracture occurs under relatively complicated stress systems a wide variety of surface markings can arise, Seldenrath and Gramberg (1958). These may be compared with those seen in the field, Roberts (1961), Hodgson (1961).

- In the elastic domain, acoustic emission occurs only when the axial load is raised above the largest value that has been reached in previous loading history.
- Question : How long does the rock keeps a memory of its past loading history ?
- How is the onset of macroscopic fracture growth defined ?

On the sources of seismic activity generated by fluid pressure variations

- $(\sigma_3 - P_0) > 0$ and Max $[(\sigma_1 - P_0)-(\sigma_3 - P_0)] <$ Elastic limit : Increase in the maximum effective differential stress : Kaiser effect; has been used as mean to estimate the rock mass hydraulic transmitivity (Shapiro et al., 1997)

- $(\sigma_3 - P_0) > 0$ and Max $[(\sigma_1 - P_0)-(\sigma_3 - P_0)] >$ Elastic limit (Modes II and III), or effective Coulomb stress ($[\tau - \mu(\sigma_n - P_0)]$ larger than fault cohesion C_0, failure in shear, eiher through a fresh plane but most often on a preexisting fault

  These are shear fractures that should generate double couple with their nodal planes inclined w.r. to fracture plane, because double couple only represents dynamic elastic response to shear stress drop during rupture.

- $(\sigma_3 - P_0) < 0$:Hydraulic fracture propagation in mode I
  - Uniform pressure P up to fracture tip :
    $K_I \propto (\sigma_{min} - P) \sqrt{\pi a}$; fracture is unstable
  - No fluid penetration, pressure P in borehole :
    $K_I \propto (\sigma_{min} - P)\ 1/\sqrt{a}$; fracture is stable

  These are tensile cracks and should generate dipoles with main axis more or less perpendicular to fracture plane; the unstable crack length is in smaller than 1 m, hence signals are very high frequency (> 100Hz)
  - The Hill mesh scheme

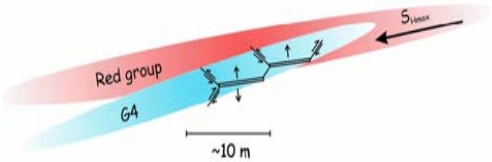

- Stress redistribution because of large scale pressure variation within the reservoir, or within the stimulated zone (also observed when pore pressure decreases).

- Resonances : long period events; tremors, trapped waves

Monitoring Seismic activity generated by fluid pressure variations

- While shear events (quadrupoles) are often in the 10 – 500 Hz range, dipoles from the crack tip are much shorter and require high frequency sensors, close to the fracture tip;
- Monitoring hydraulic fractures requires downhole instrumentation and a few companies have specialized in this operation
- Presently work is under progress to retrieve signals from surface sensors

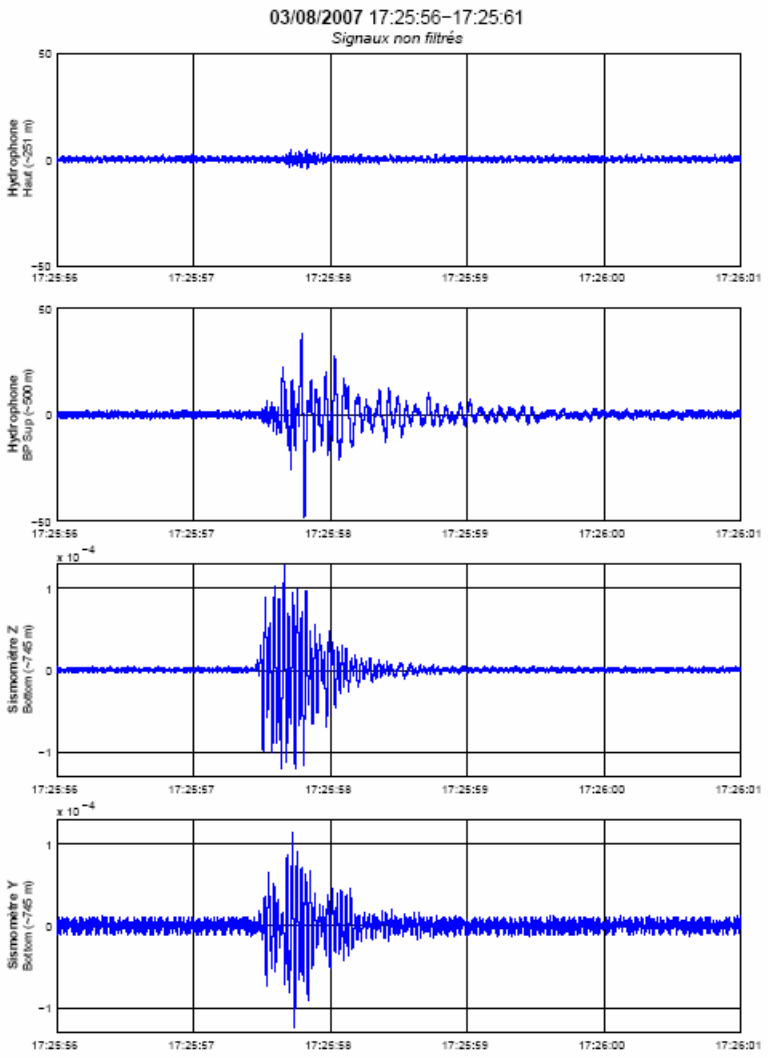

Determination of the regional stress field

Main techniques :

- From cores, because rocks are visco-elstic and keep some memory of past loads;
- From underground cavities (flat jacks, overcoring)
- From boreholes (overcoring, hydraulic testing, boreholes wall failure analysis)
- From focal mechanisms
- From seismic anisotropy

Stress determination from Hydraulic Fracturing

- Hydraulic Fracturing
  - Valid only if borehole is parallel to a principal stress direction.
  - Frac orientation yields maximum Horizontal principal stress direction
  - Shut in pressure (stabilization of pressure when injection stops) yields minimum horizontal principal stress magnitude
  - Breakdown pressure yields maximum Horizontal principal stress magnitude
  - But problem for taking into account pore pressure in breakdown equation and difficulty for determining “tensile strength”

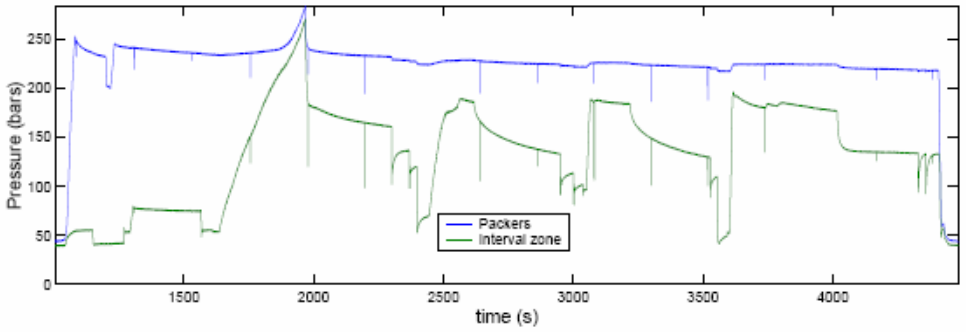

$$\sigma_{\theta\theta} = -\sigma_H + 3\sigma_h - P_w + \sigma^T$$

Ultrasonic Borehole imaging of Hydraulic fracture

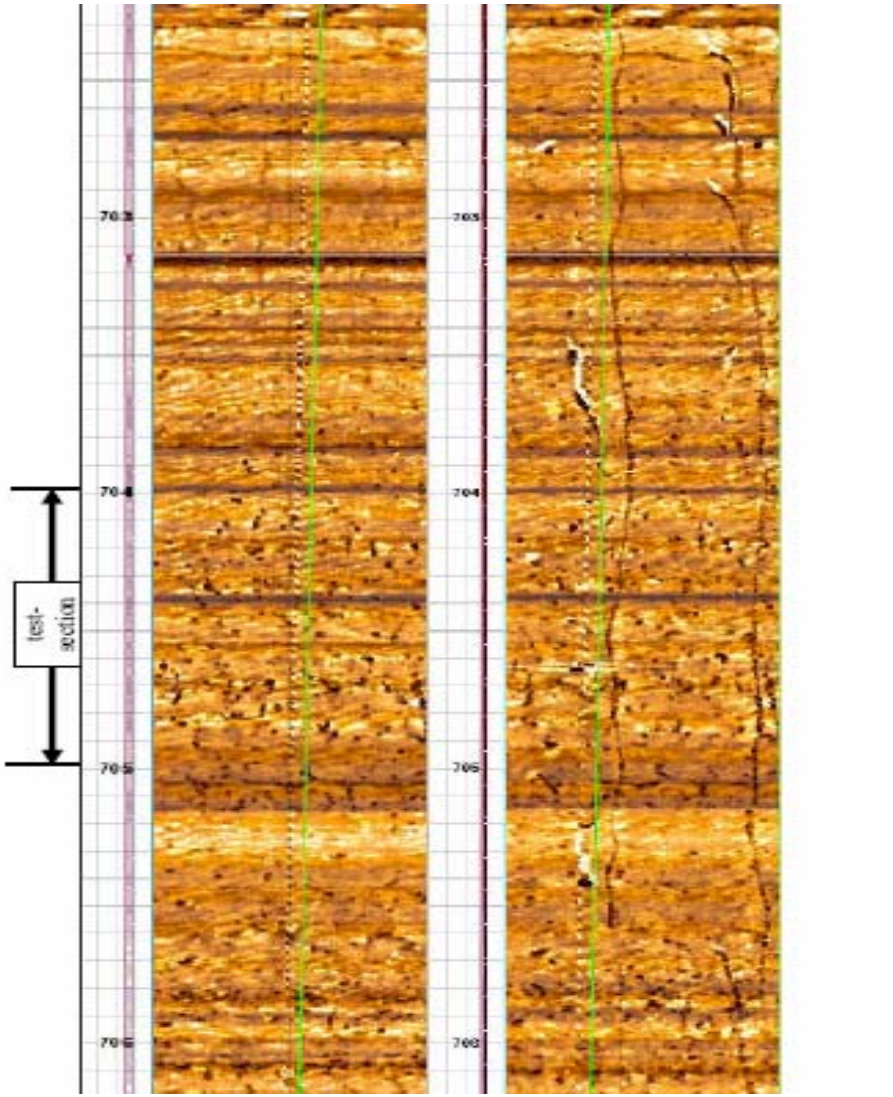

Ultrasonic Borehole Image (UBI) of a hydraulic fracture. On the left before testing (no fracture seen), on the right after hydraulic testing : the logging shows the vertical fracture that extends, in this case, beyond the packed off interval.

Imaging logs (electrical or ultrasonic), provide much longer borehole coverage than traditional impression packers and help determine whether the fracture remained constrained in the packed off interval

Stress determination from Reopening preexisting fractures (HTPF)

- Preliminary electrical imaging log yields images of « preexisting » fractures
- Hydraulic testing on preexisting fracture yields normal stress supported by corresponding fracture : $\sigma_n = \sigma \, \mathbf{n} \, . \, \mathbf{n}$
- If more than 6 different directions are tested, then the 6 components of σ may be determined
- In practice integrate HF and HTPF : 3 to 4 HF tests yield direction and magnitude of minimum principal stress while 2 to 3 HTPF tests yield magnitude of other principal stress components
- But problem with quasistatic reopening tests if fracture is inclined to borehole direction; Hence better use only shut-in pressure tests

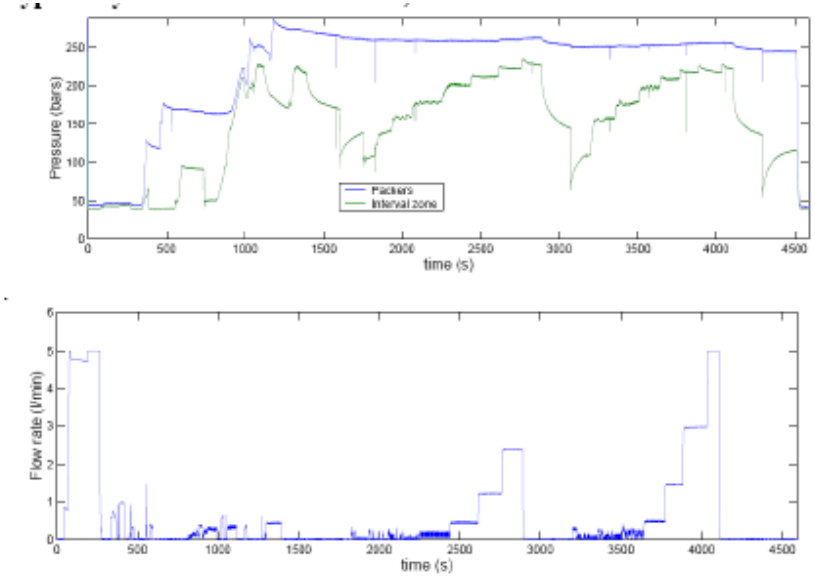

$$\sigma(x_3) = \sigma(x_c) + (x_3 - x_{3c})\,\alpha$$

Stress determination from borehole failure analysis

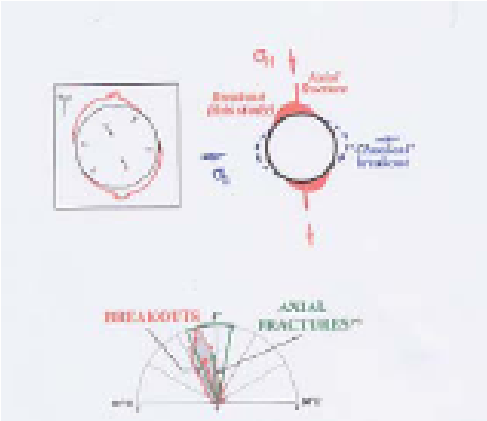

- Tangential stress at the borehole wall

$$\sigma_{\theta\theta} = (\sigma_h + \sigma_H) - 2(\sigma_H - \sigma_h)\cos 2\theta - P_b - f(P_0) - \alpha E \Delta\theta / (1-\nu) - 3/8\ \Delta\alpha E/(1-\nu)\ \Delta\theta$$

Where $\Delta\alpha$ is the mismatch between thermal expansion coefficients (solution for square inclusion in an homogeneous matrix)

- Time dependency of cooling :
  - Slow cooling yields borehole elongation (thermal breakouts),
  - fast cooling yields macroscopic thermal cracking

Breakouts and tensile induced fractures are well detected with borehole imaging tools such as the Ultrasonic borehole imager or the Electrical Formation Imager.

Ultrasonic imaging (UBI)

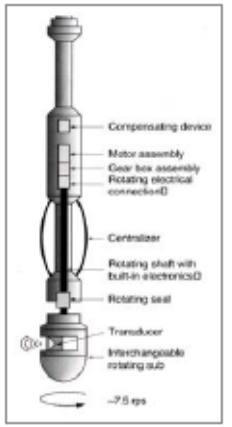

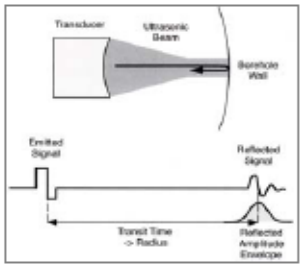

Information from double couple focal mechanisms

- **Data produced by fault plane solutions**

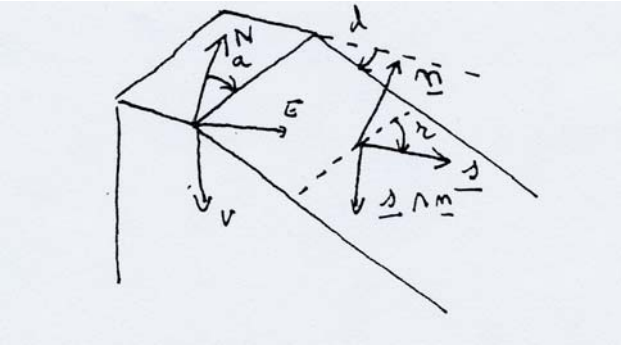

- Focal mechanisms of pure shear faults (no significant dilatancy), yield for both nodal planes the dip and azimuth of the plane (d and a) as well as the slip direction in the plane (rake angle r of slip vector **s**) when it corresponds to the fault plane
- (a1, d1, r1, εa1, εd1, εr1 , a2, d2, r2, εa2, εd2 , εr2).

- **Principle of inversion** : **s** . τ **/ |**τ**|** = 1

τ Resolved shear stress in plane

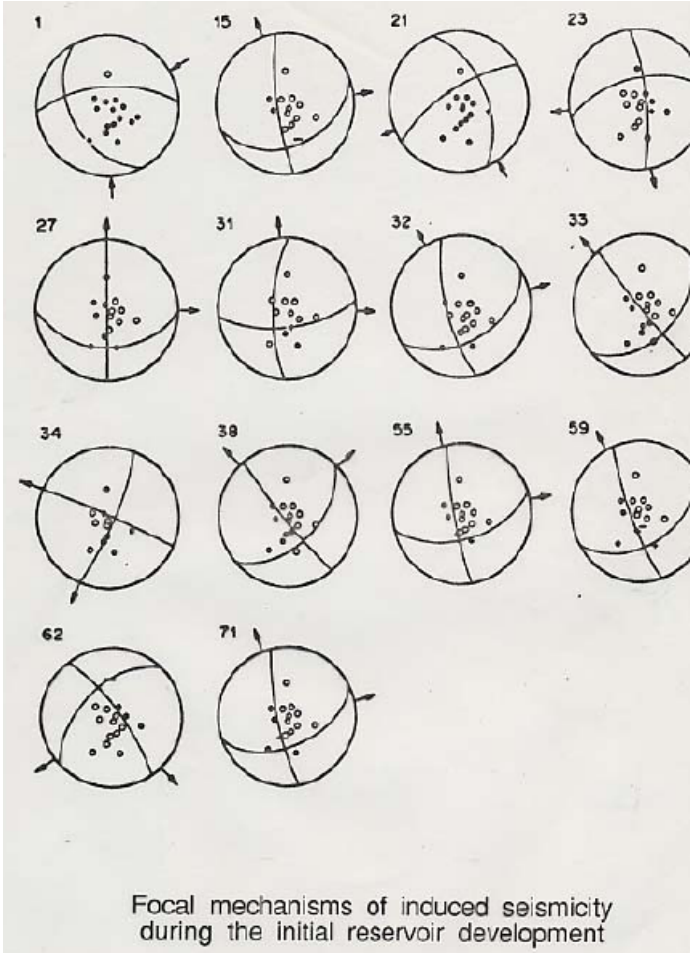

Focal mechanisms of induced seismicity during the initial reservoir development

Gephart & Fosyth's approximate method – 1

Gephart and Forsyth, JGR, 1984

- Basic assumptions
  - Slip occurs parallel to the direction of the resolved shear stress.
  - All seismic events are distant enough from each other so that the stress perturbation induced by each event does not alter the stress field for other events.
  - The original stress field is uniform within the volume sampled by the various events

- The stress is decomposed as :

$\sigma = \sigma 1\ \mathbf{I} + (\sigma 3 - \sigma 1)\ \mathbf{T}$

In which T has the same principal directions as σ and O, R and 1 as eigen values, with

$R = (\sigma 2 - \sigma 1) / (\sigma 3 - \sigma 1)$

- We consider two frame of reference, Q corresponds to the eigen vectors of **T,** and Q' is associated with the fault plane (normal **n**, slip vector **s** and **n^s**).

- For tensor T to be compatible with a given slip vector in a given fault plane, it is necessary that :

$$R = - \beta_{13}\, \beta_{23} \ / \ \beta_{12}\, \beta_{22}$$

Where β_{ij} are the components of the orthogonal tensor that rotates Q to Q'

The idea is to explore the set of all possible solutions and to identify that which fits best observations, namely the tensor that yields resolved shear stress directions closest to observed slip vector directions.

But uncertainties exist on all angles.

The problem is three folds :

- Identify for each focal mechanism which nodal plane is the fault plane;
- For all focal mechanisms define a measure of their misfit with a given tensor **T.**
- Identify the best solution and associated confidence level domains.

Gephart & Fosyth's approximate method - 2

- Identification of fault planes and measure of misfit
  - For any given nodal plane, identify smallest rotation of plane required to bring **s** parallel to τ
  - For a given tensor **T,** chose as fault plane, for each focal mechanism, that which requires the smallest rotation.
  - Characterize the misfit, for the corresponding tensor **T,** by the quantity (L1 norm) :

$$m_i = \sum_{k=1}^{N} \min(x_k^l, l = 1,6)$$

X_k^l is the l^{th} rotation for focal plane solution k.

- Identification of solution : given $0 \leq R \leq 1$, and given Euler angles range from 0 to 360°, the complete domain of possible solutions is explored. The solution is that which yields the smallest misfit.

- 64% and 90% confidence level with L1 norm complete the characterization of the solution

Table 1

Expressions for rotations about axes of fault plane geometry.

Rotation axis	Algorithm	Period
n	$\theta = -\tan^{-1}\left[\frac{RB_{12}B_{22} + B_{13}B_{23}}{RB_{12}B_{32} + B_{13}B_{33}}\right]$	Π
s ∧ **n**	$\theta = \tan^{-1}\left[\frac{RB_{12}B_{22} + B_{23}B_{13}}{RB_{22}B_{32} + B_{23}B_{33}}\right]$	Π
s	$\theta = \frac{1}{2}\tan^{-1}\left(\frac{2}{k}\right)$ where $k = \frac{R(B_{12}^2 - B_{22}^2) + B_{13}^2 - B_{23}^2}{RB_{12}B_{22} + B_{13}B_{23}}$	$\frac{\Pi}{2}$

- The problem with a large ERV

$$\sigma(x_3) = \sigma(x_c) + (x_3 - x_{3c})\,\alpha$$

$$R = (\alpha_2 - \alpha_1) / (\alpha_3 - \alpha_1)$$

Principal stress directions and shear wave splitting

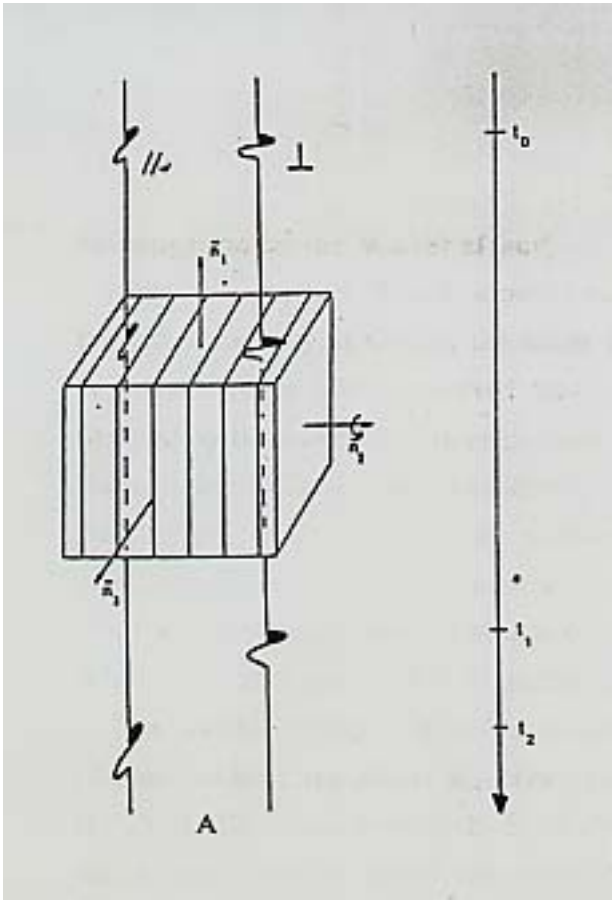

- When rock mass is anisotropic, two shear waves arrivals are detected; their polarization occurs in two perpendicular directions.

- When rocks support a non hydrostatic stress field, the maximum principal stress direction corresponds to a larger Young's modulus than the direction of the minimum principal stress. This results in shear wave splitting, the fastest arrival being in coincidence with maximum principal stress direction.

Two examples of fluid induced seismicity

1. The Soultz/Forêts experimental geothermal site in the Rhine Graben (France)

2. The swarm activity in the Corinth Rift (Greece)

The European Experimental Hot Dry Rock site at Soultz

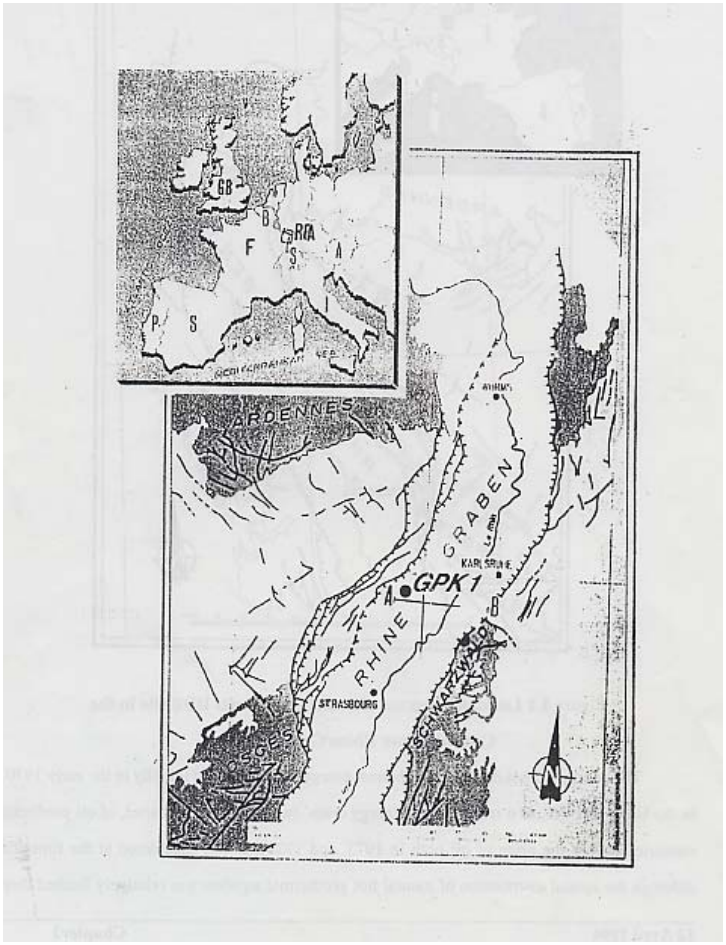

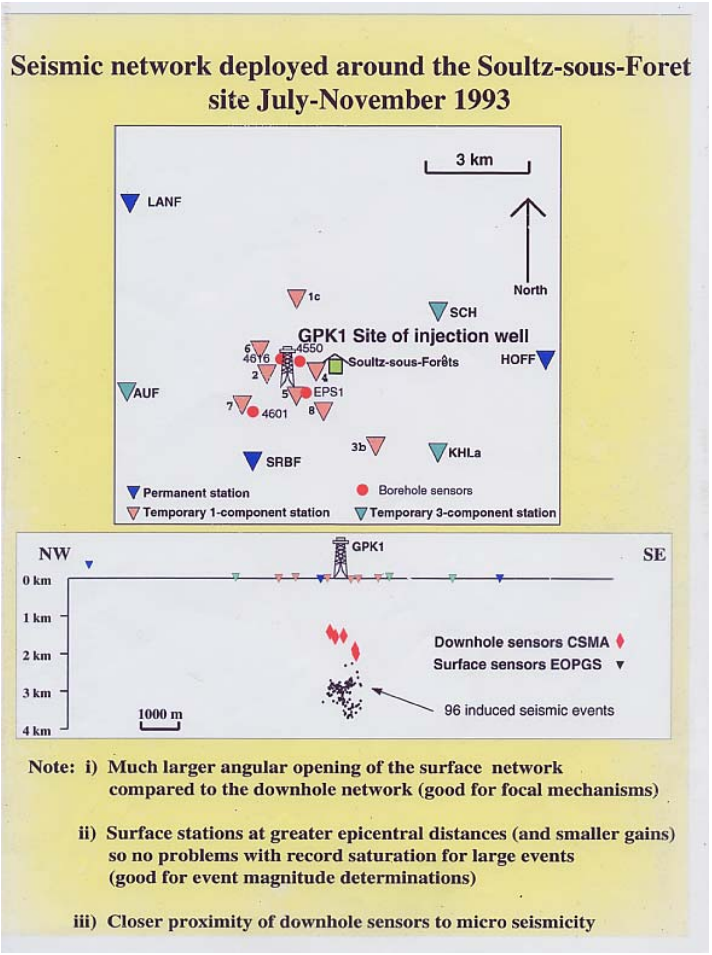

Principles of reservoir development

Today realisation

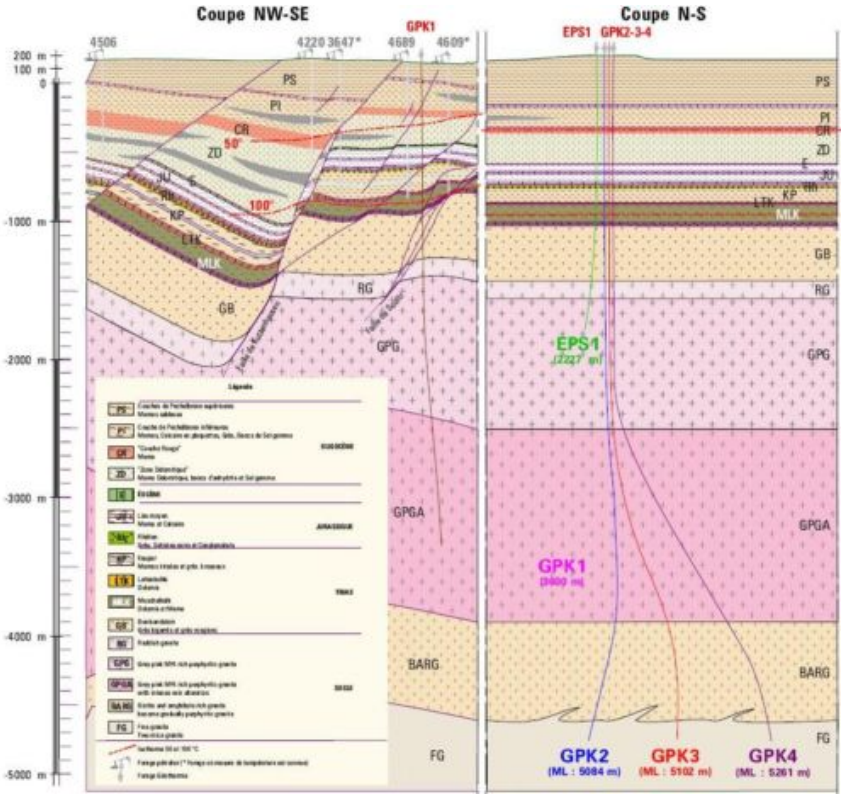

Initial goals

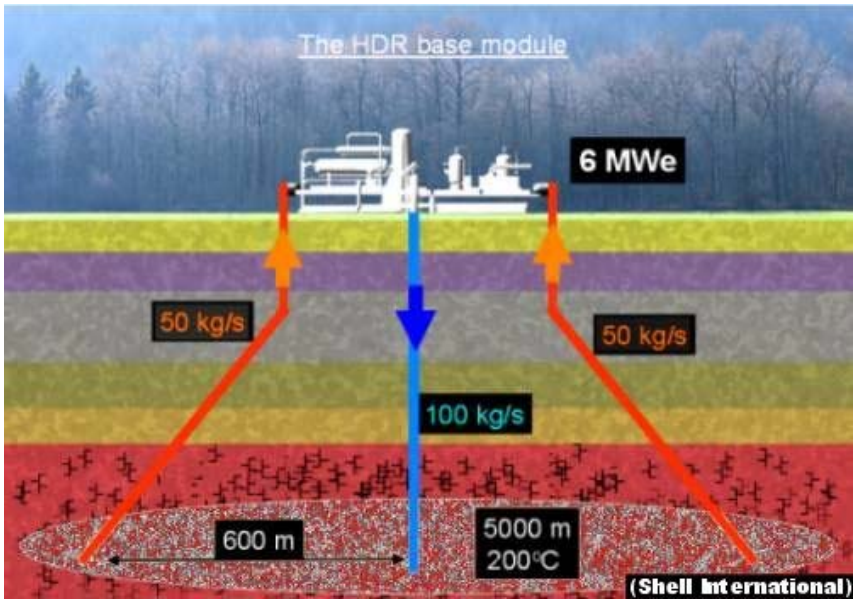

Compression breakouts observed in well GPK1 around 3440 m

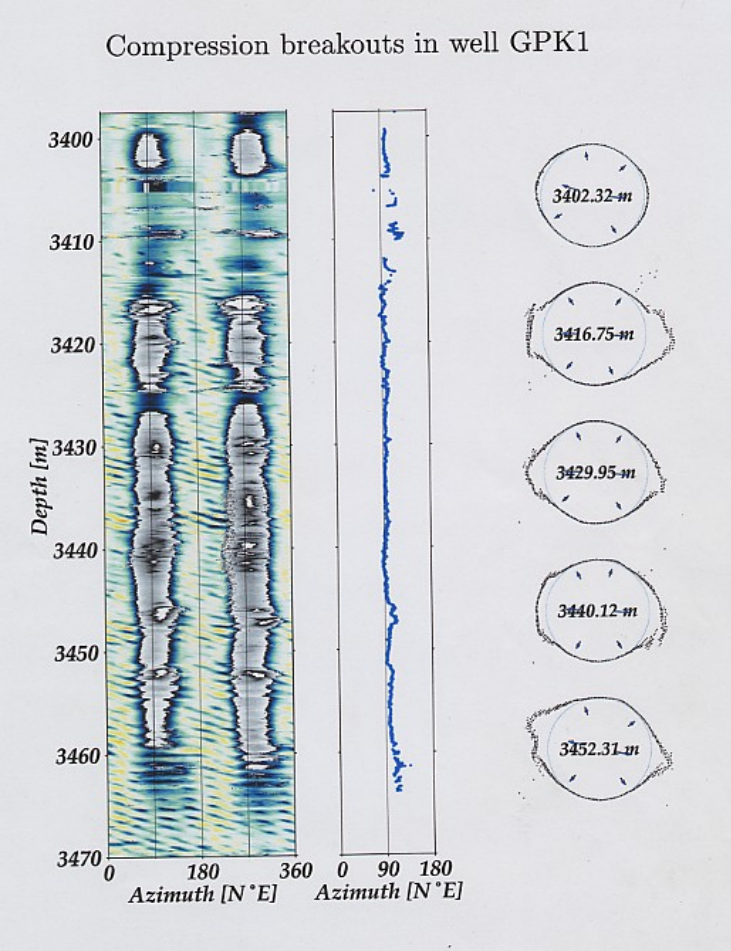

- Compression breakouts are indicative of zones of highest tangential compressive stress :

  $-\sigma_h + 3\,\sigma_H - P_b - f(P_0) - \alpha E \Delta\theta / (1-\nu) = \sigma^c$

- No breakouts seen initially in GPK1, No breakouts in GPK2 just after drilling, some seen sometime after drilling : problem of time dependency for breakout development.

- Recall loading rate effect on rock strength (e.g. Hudson & Brown, 1973)

Variation with depth of thermal perturbation in well GPK2

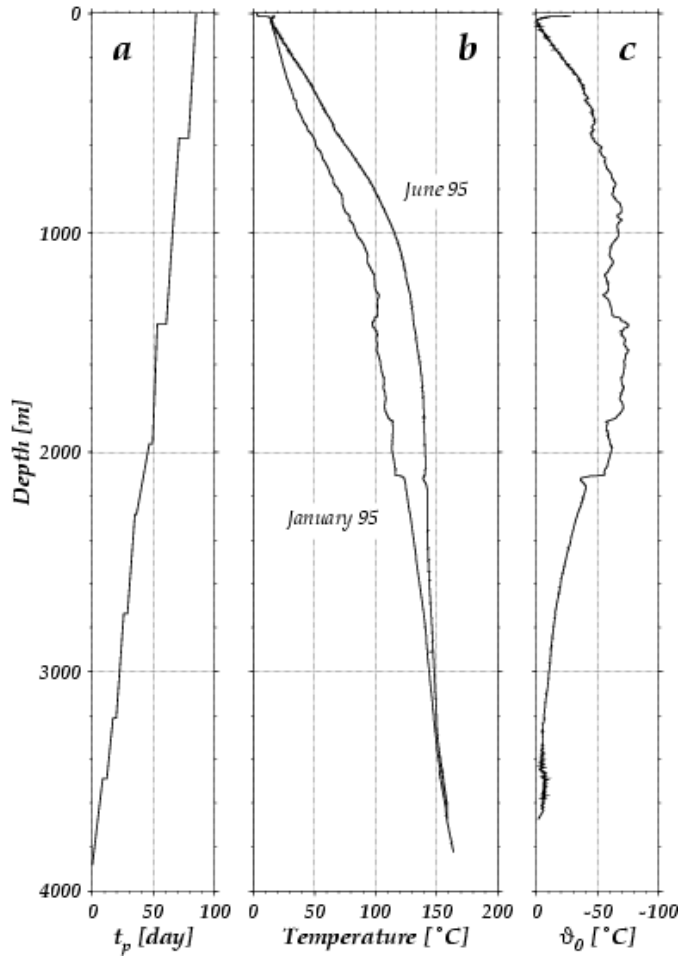

- a) Time of exposure to drilling mud circulation
- b) Thermal recovery after drilling :
  - January 95 is 3 days after the end of drilling
  - June 95 may be considered close to equilibrium (129 days after well completion)
- **C)** Variation of temperature perturbation with depth. Can it be used for stress magnitude determination ?
- On the problem of time dependency and stress corrosion on “strength” :
  - In tension
  - In compression

Analysis of drilling induced fracture

Result with electrical imaging (FMI) tool

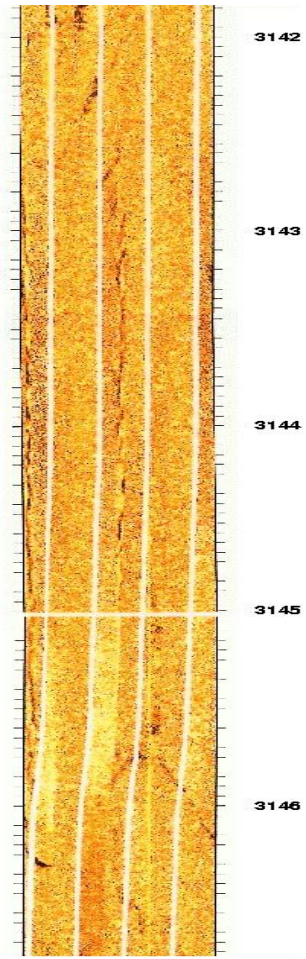

- drilling Induced fractures : thermal cooling caused by drilling

  $-\sigma_H + 3\,\sigma_h - P_b - f(P_0) - \alpha E \Delta\theta / (1-\nu) = \sigma^T$
  Where $\Delta\theta$ is the cooling of the rock

- From a Bore HoleTeleViewer (BHTV) log run in GPK1 down to 2000 m, Mastin and Heineman (1988) determine a mean direction for drilling induced fractures = N 169° ± 7°

- From FMI log run from 1500 m down to 3500 m, Brudy and Zoback find that the mean orientation of drilling induced fractures is N 181 ± 22 °

Borehole elongation observed in well GK2 between 1600 m and 2900 m

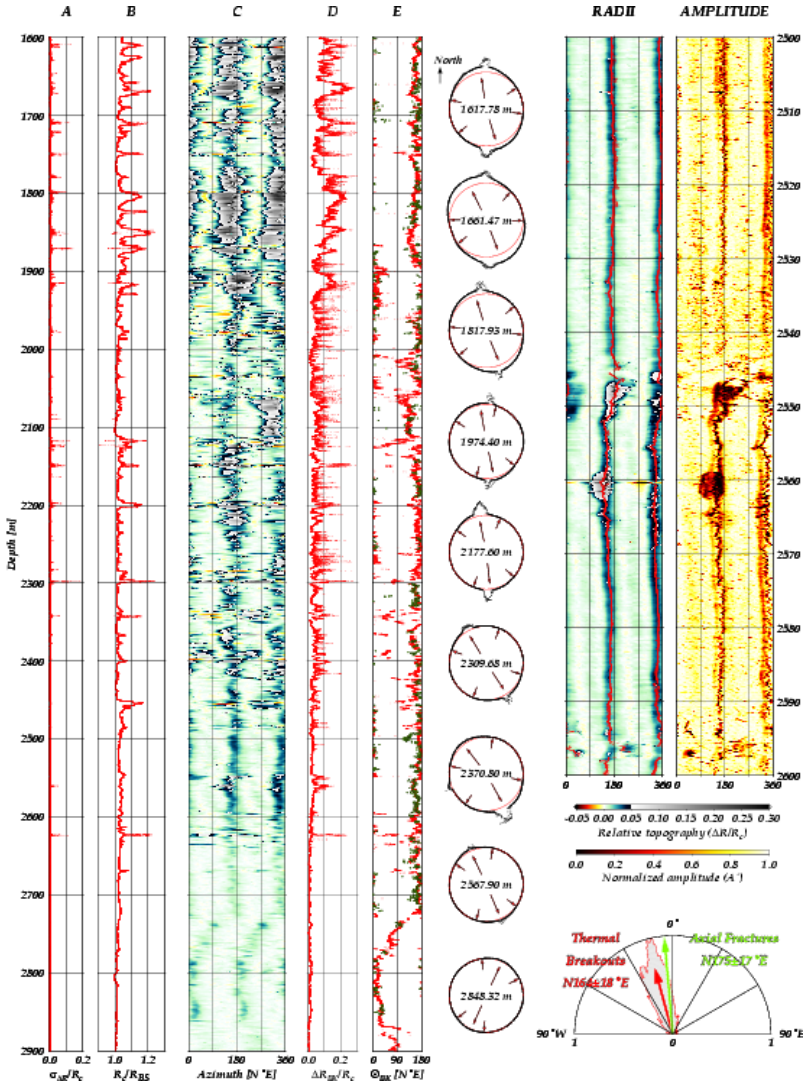

Results from large scale hydraulic reconnaissance test (2850-3400 m) (Sept. 1993)

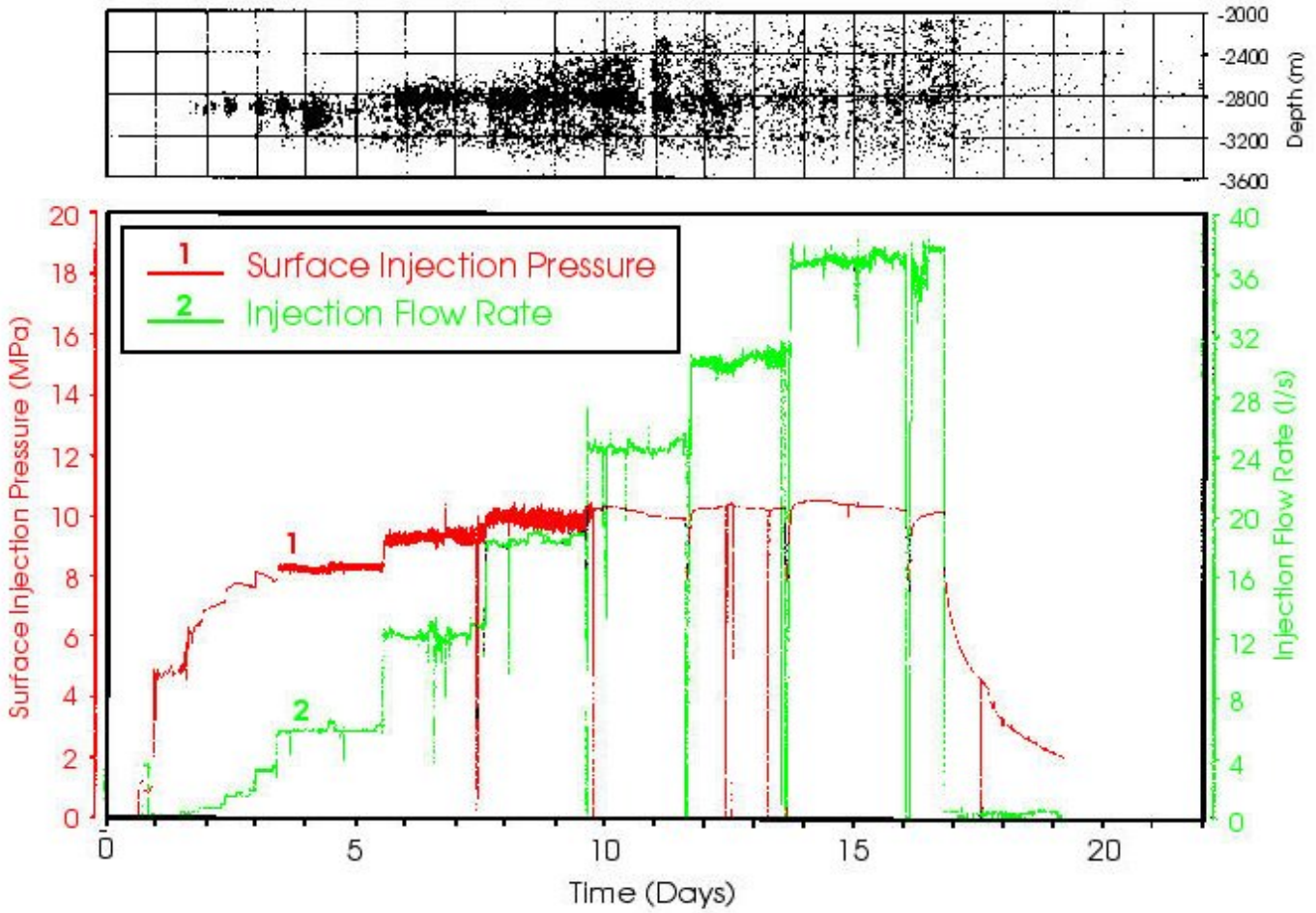

Location of induced microseismic events

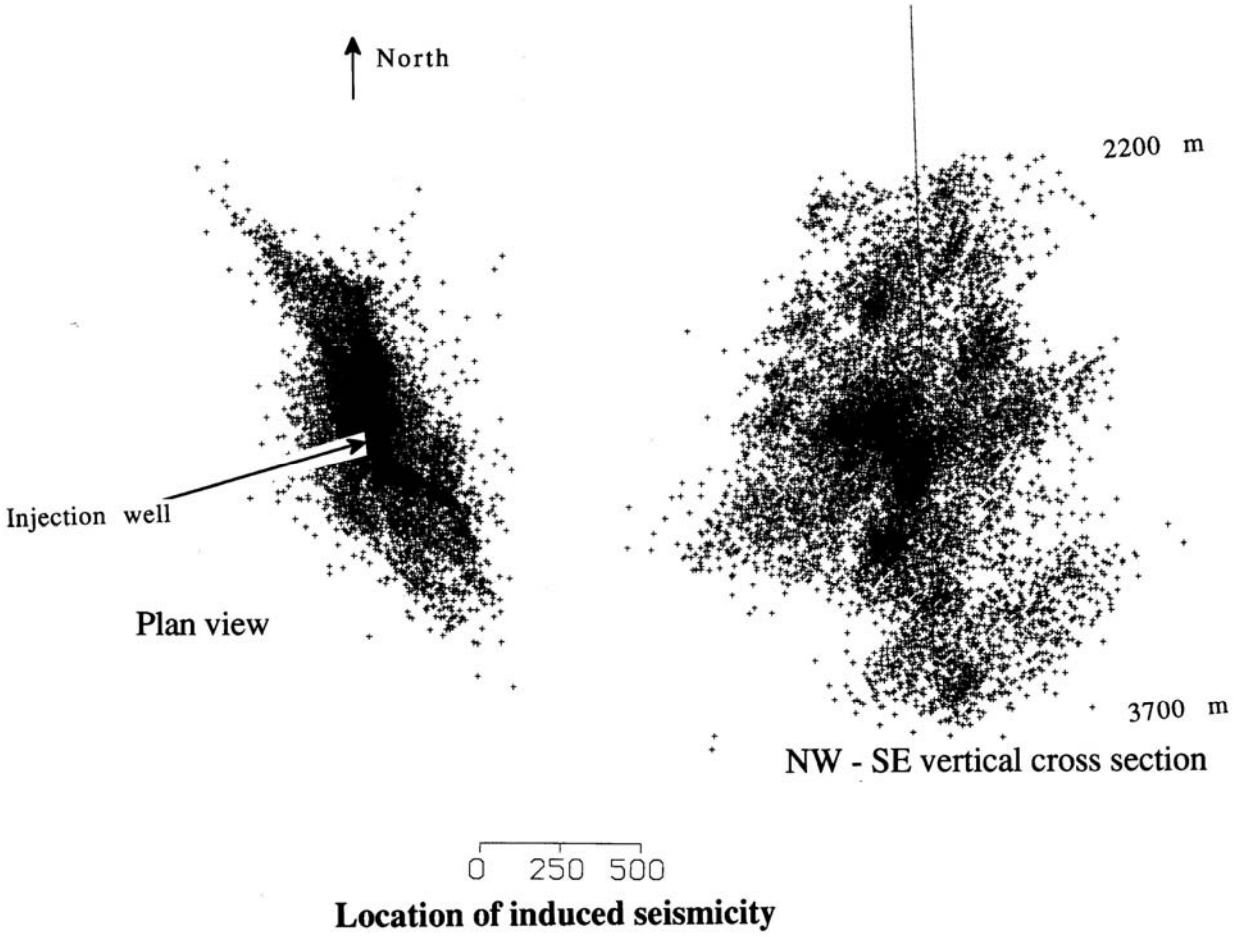

Closer analysis of horizontal direction of microseismic cloud

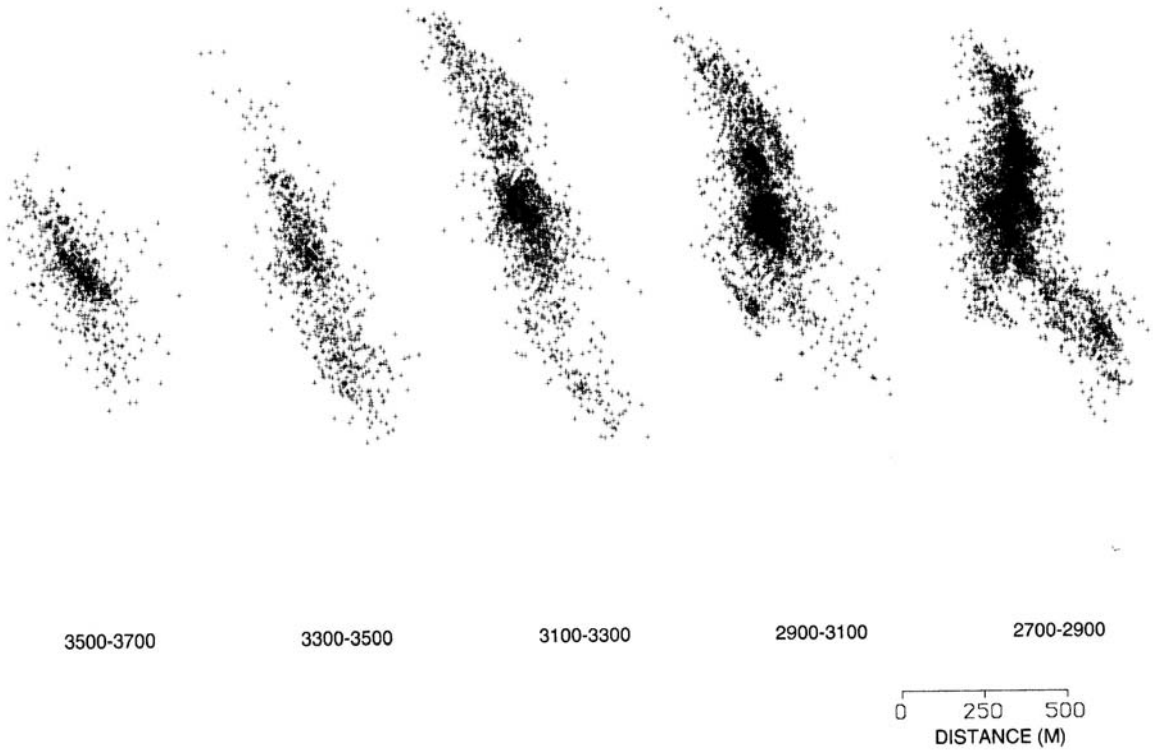

Evaluating the regional stress field

- Mean stress direction and local heterogeneity :
  - On the role of faults on stress reorientation
  - How valid is the rock mass continuity hypothesis
  - Consequences for focal plane inversions

- Stress magnitudes evaluation
  - Vertical stress component
  - Minimum principal stress magnitude
  - Maximum principal stress magnitude

Heterogenity in stress direction

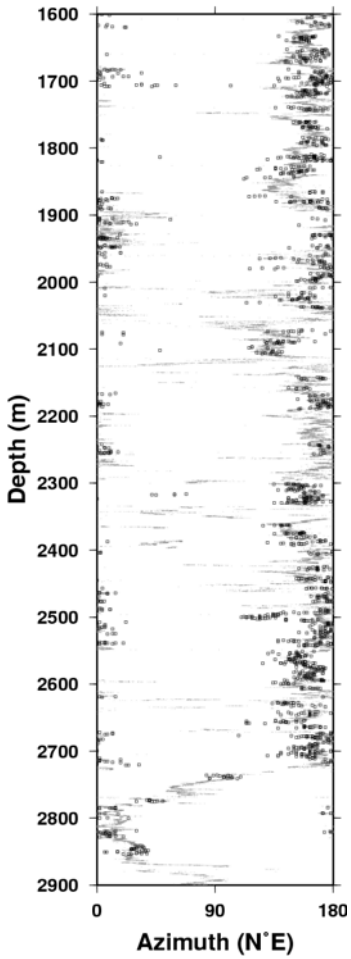

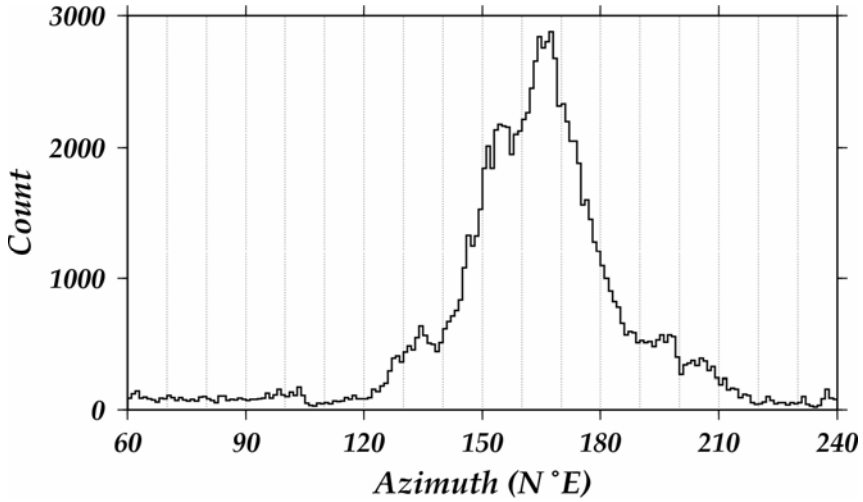

Analysis of fault plane solutions from induced microseismicity

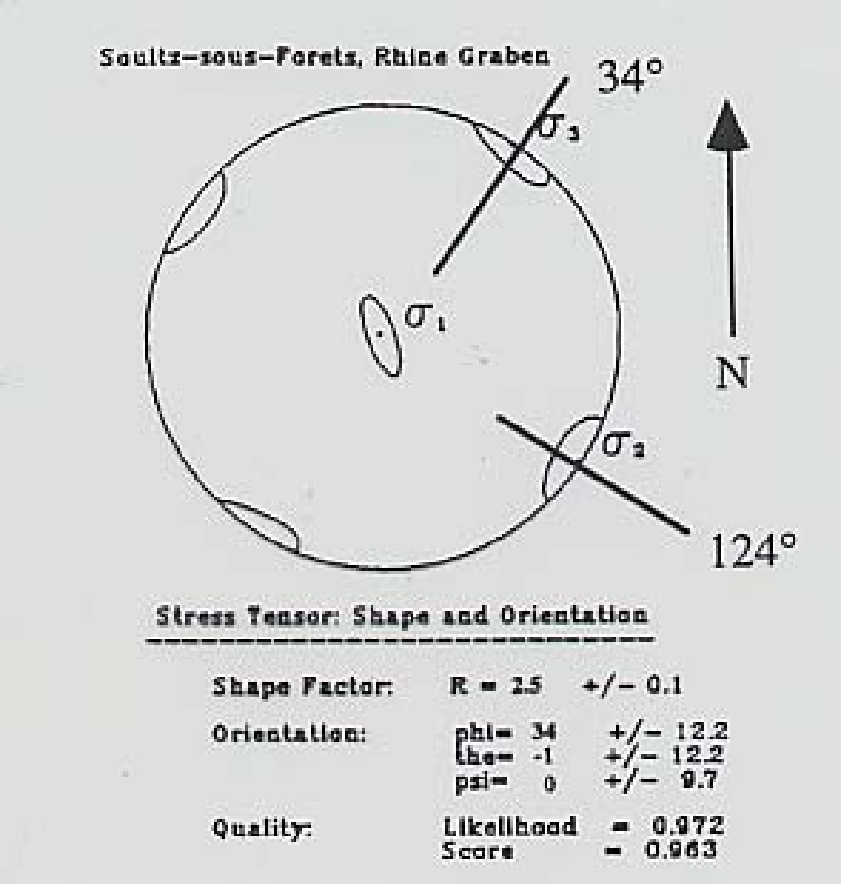

- 2 nodal planes for each focal mechanism
- Slip vector **S** in nodal plane is parallel to resolved shear stress τ in nodal plane

  S . τ / | τ | = 1

  τ = Tn – (Tn.n)n

$$(\sigma) = \sigma_1(1) + (\sigma_3 - \sigma_1)\begin{pmatrix} 0 & & \\ & 1 & \\ & & R \end{pmatrix};$$

$$R = (\sigma_2 - \sigma_1)/(\sigma_3 - \sigma_1)$$

Focal mechanisms and stress directions

- Stress perturbation caused by previous events

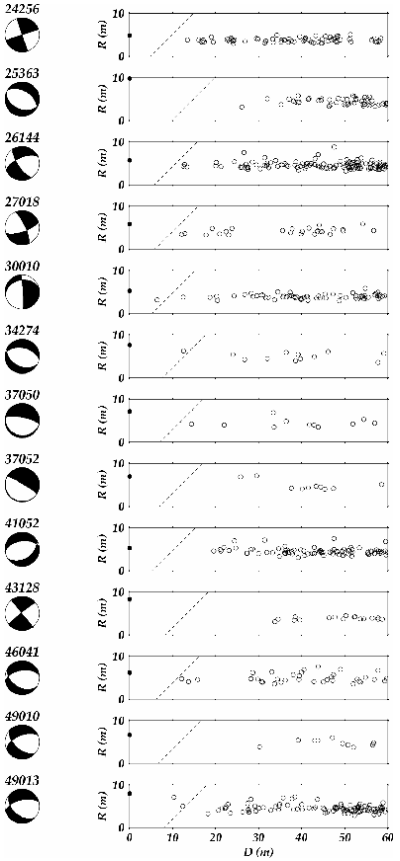

- Characterization of preexisting stress heterogeneity

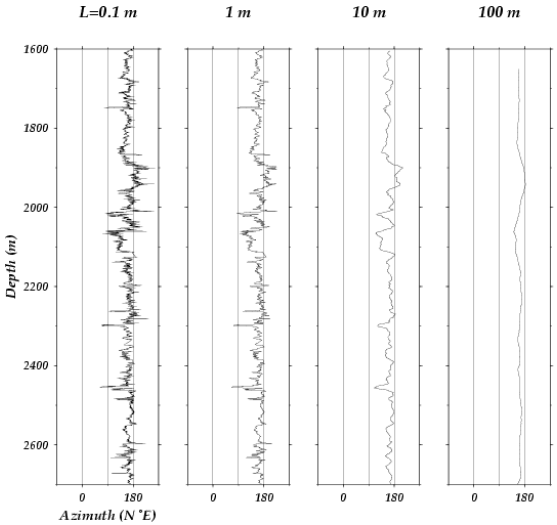

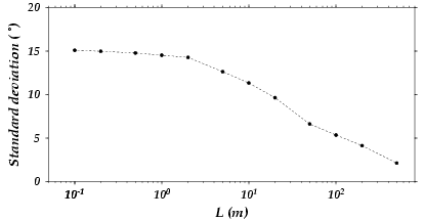

Principal stress direction determination from shear wave splitting analysis

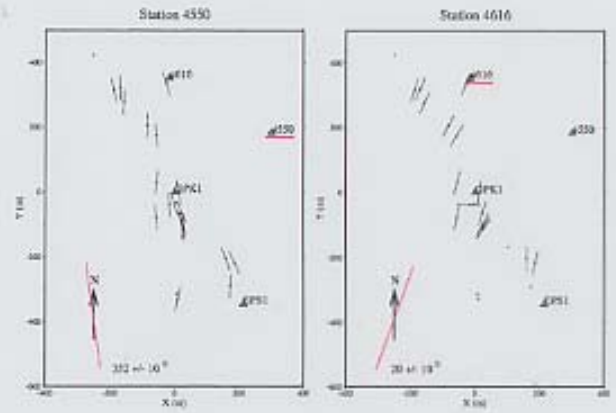

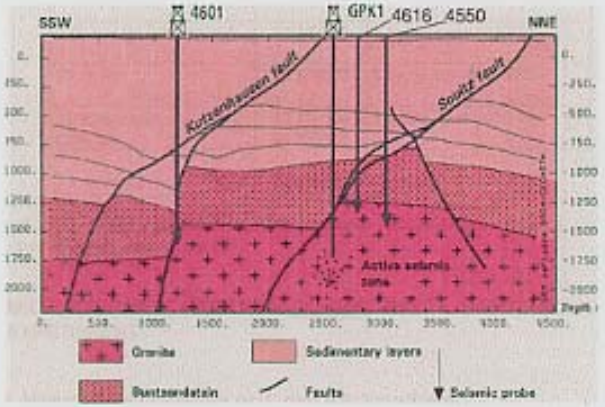

- S wave splitting

⇐ hexagonal anisotropy with a N-S horizontal symmetry axis, consistent with σ_H

- Stress rotation

⇐ topography of the sediment-granite boundary

Comparison with other regional stress determination

- Results from Urach, from borehole breakouts between 1900 m and 3500 m (Heinemann et al., 1992) : N 172 ± 17°N

- Results from KTB (Brudy et al., 1999)
  - Hydraulic fractures down to 3000 m : N 149°± 15
  - Drilling induced fractures from 3000 m to 4000 m : N 154°± 17
  - drilling induced fractures from 3000 to 6000 m : N 166° ± 17°
  - Drilling induced fractures at 7000 m : N 182°± 21
  - Drilling induced fractures at 7 800 m : N 177°± 11°
  - Borehole breakouts in the upper part of well : N 149° ±18°
  - Borehole breakouts around 8000 m : N 171° ± 17

Flow rate measurements during the test

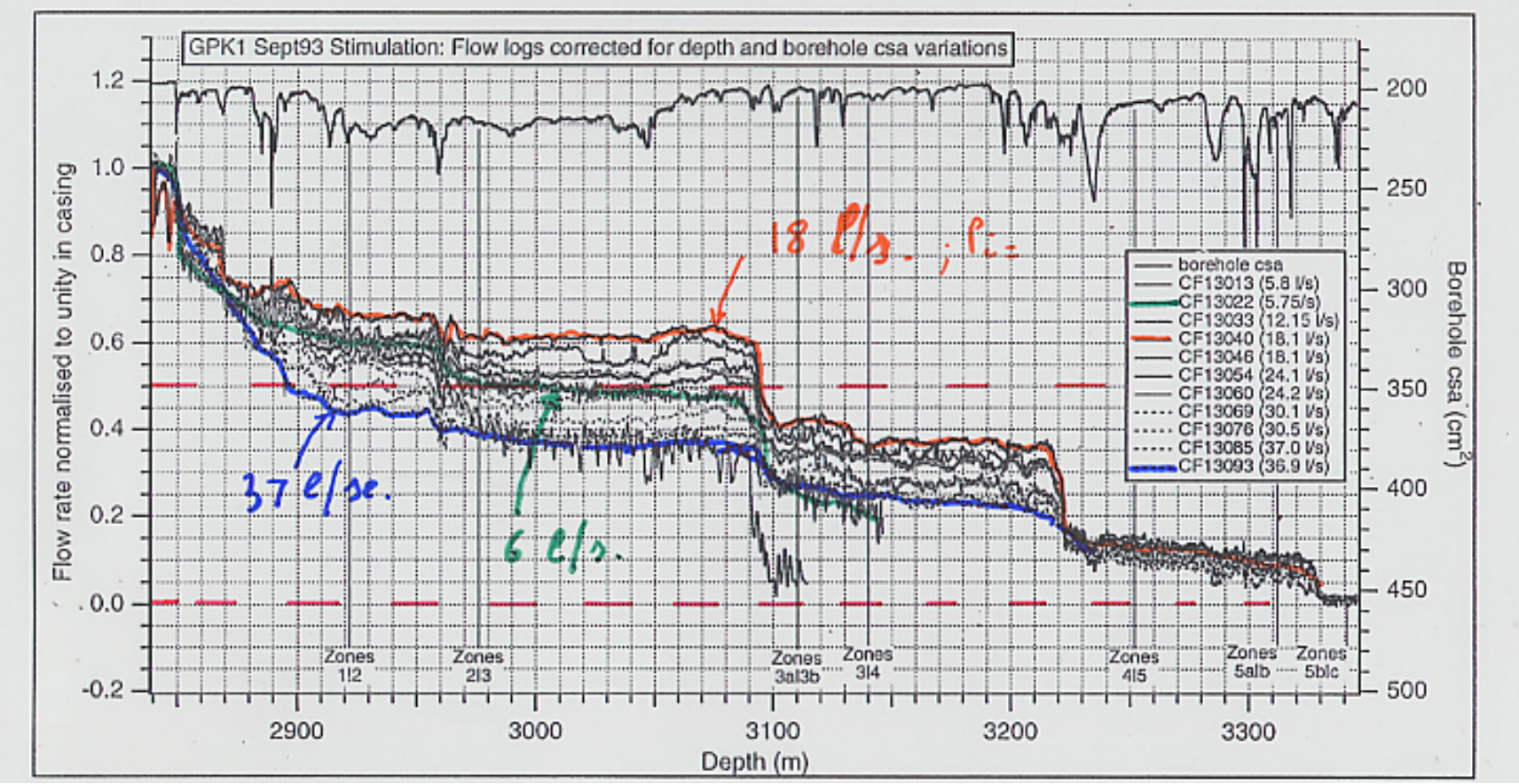

Fluid flow and induced seismicity

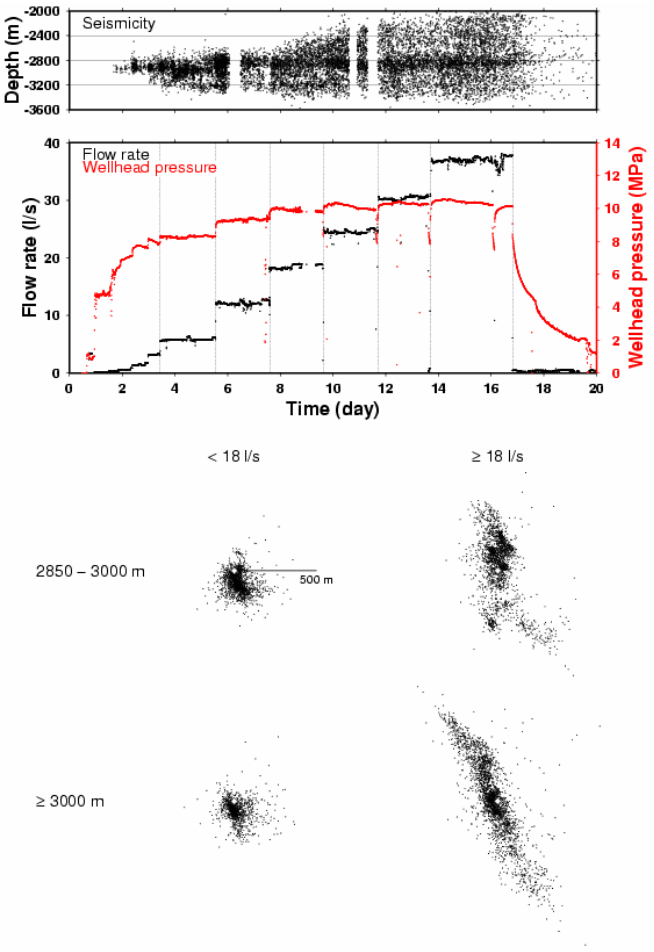

Seismic activity and hydraulic characterization of rock masses

Shapiro et al's proposition for determining the hydraulic diffusivity of a rock mass from the rate of growth of the seismic cloud :

Hypothesis : seismicity is triggered by pressure variation so that rate of growth of cloud linked to pore pressure diffusion process by :

$$\partial P/\partial T = D\,(\partial^2 P/\partial x^2 + \partial^2 P/\partial y^2 + \partial^2 P/\partial z^2)$$

A solution is sought for a step function point source so that radius r of cloud at time t is given by :$r = \sqrt{(4\pi\ Dt)}$

The rate of growth of the pressure front follows a parabola

Evaluation of the rock mass permeability from the rate of growth of the microseismic cloud (Shapiro et al., 2000) yields pore pressure at time of failure inception

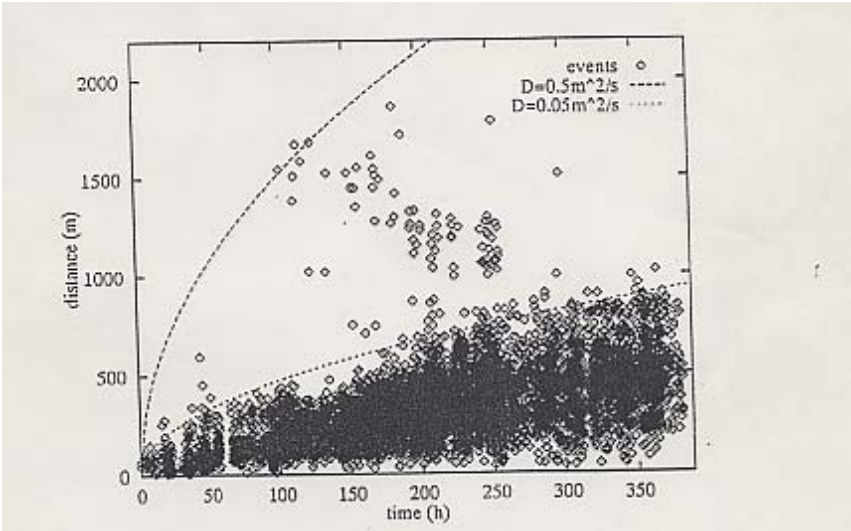

Conclusions from Soultz

- On principal stress directions at depth (below 2000 m) :
  in western central Europe : N 170 ± 10 E

- On inversion of focal plane solutions : beware local stress heterogeneity (source size > 50 m).

- On vertical stress profile : linearity probably does not come friction, since rock mass is not at failure. It comes possibly from a visco-elastic behavior linked to pressure solution.

- Rock mass hydraulic characterization may be derived from the rate of growth of the seismic cloud only if rock mass remains in the elastic domain (application of Kaiser effect)

New results and challenges for the Corinth Drilling Project

François Henri Cornet
CNRS-INSU & IPG-Strasbourg

Geodynamic background

Seismic activity in the Corinth Rift zone and the Corinth Rift Lab (CRL)

The AIG10 well and its permanent instrumentation

New challenges

Influence of roll back in the Aegean area

from L. Royden, 2007

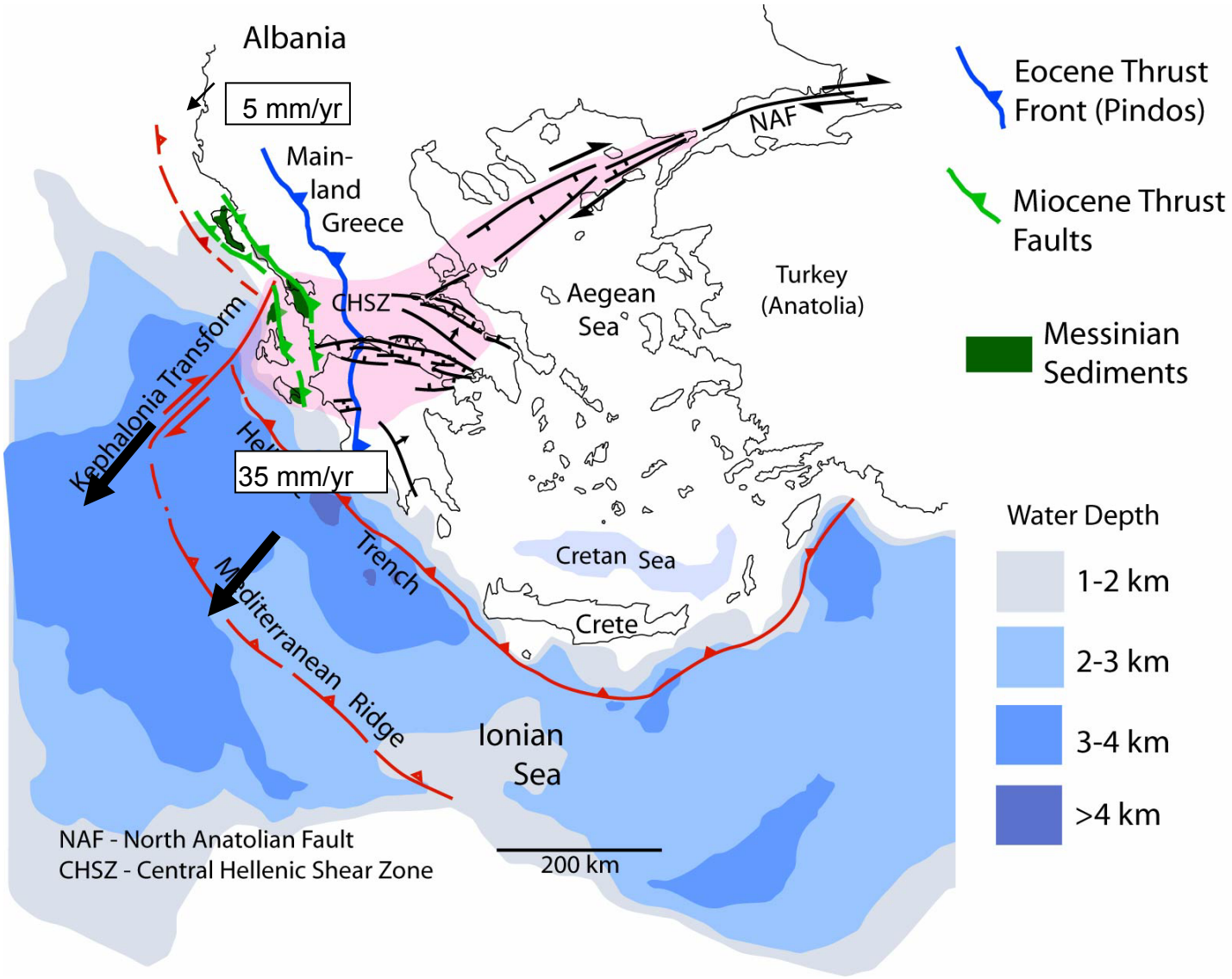

Seismic activity in Greece 1970-2007

- Cumulated energy

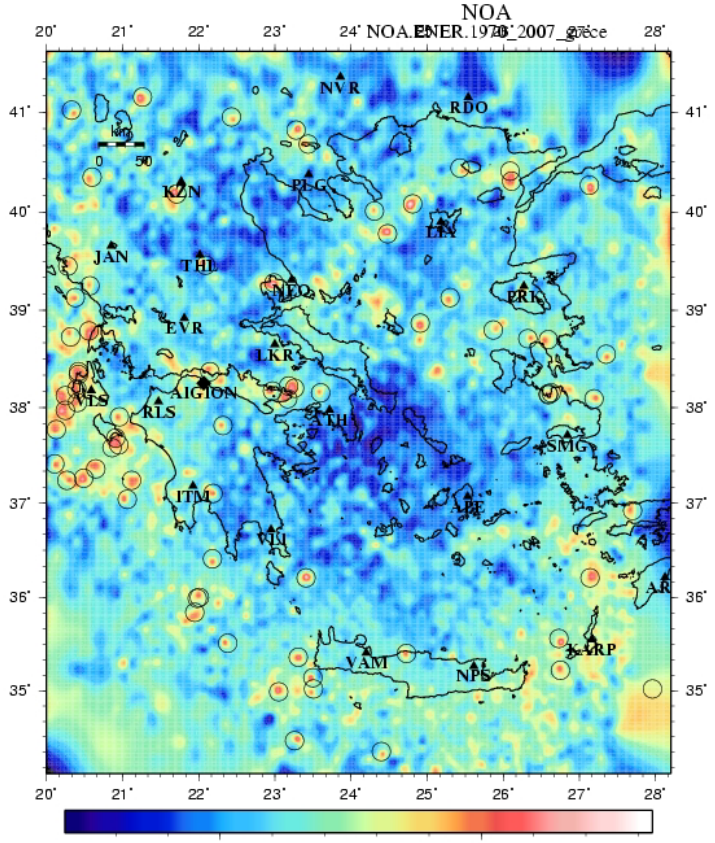

- Nb of events

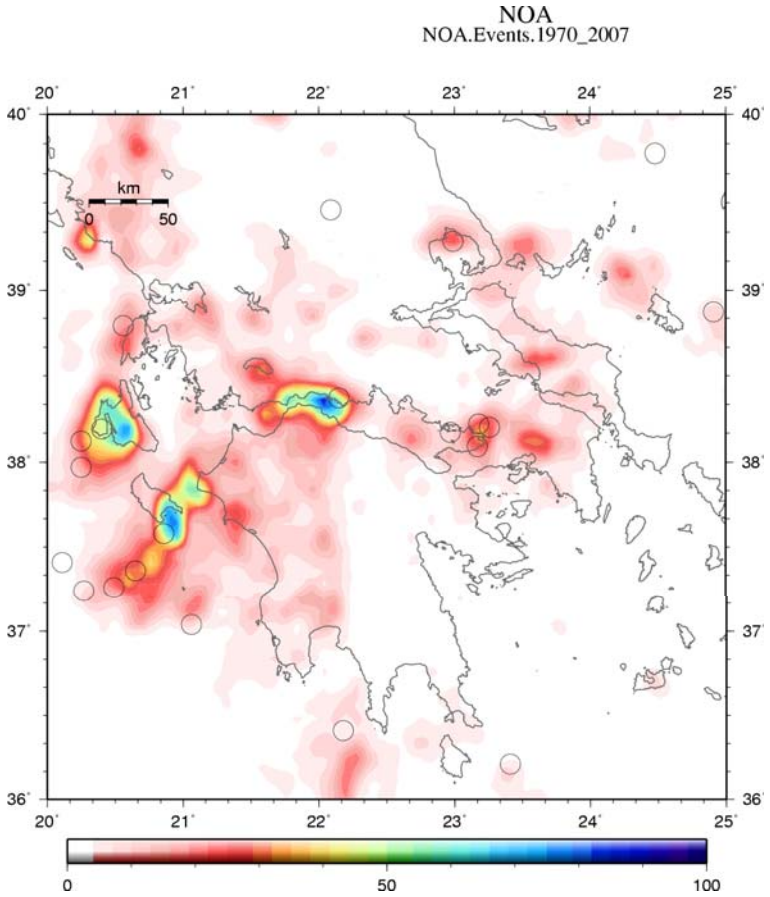

Structural cross section as defined in 1996

(Rigo et al., 1996, Lemeur et al. 1994)

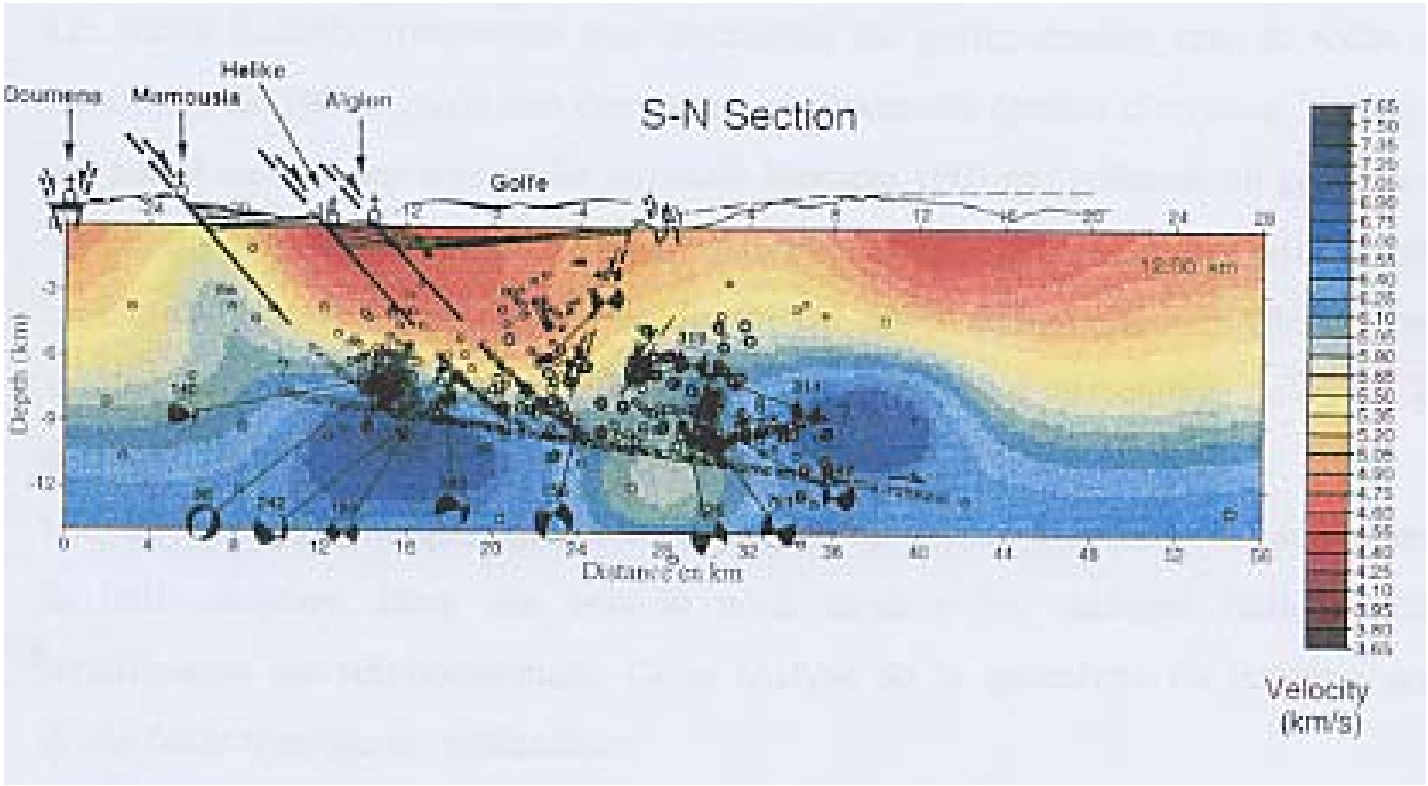

2000-2007 Seismicity
Automatic Detection

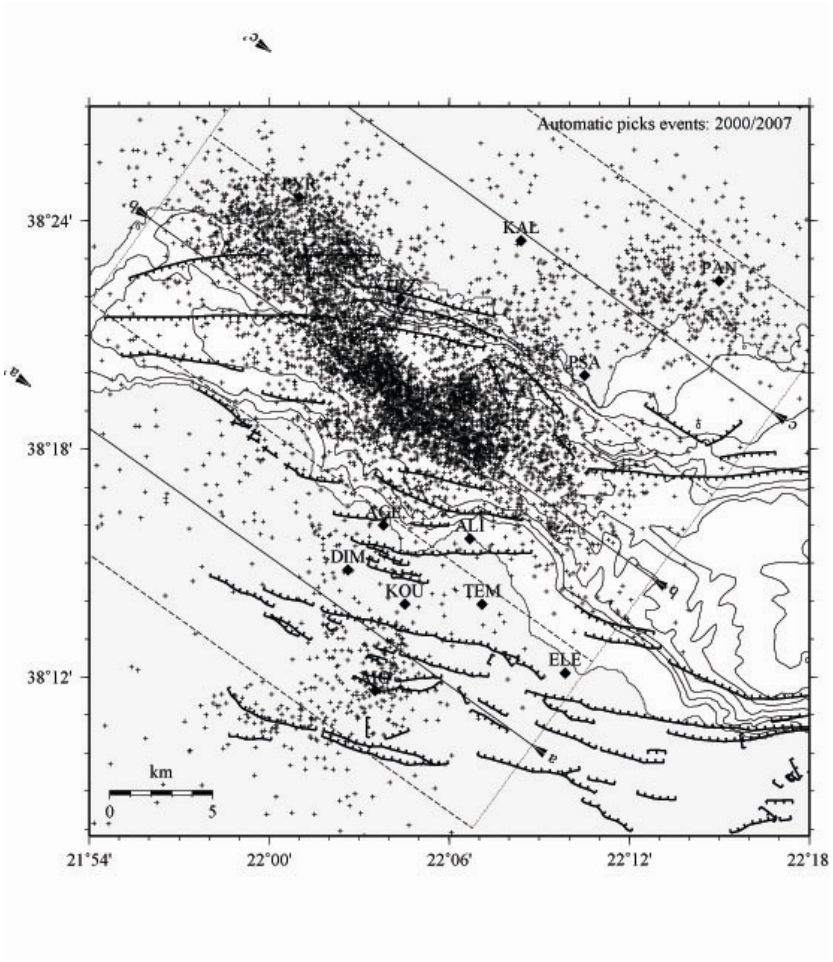

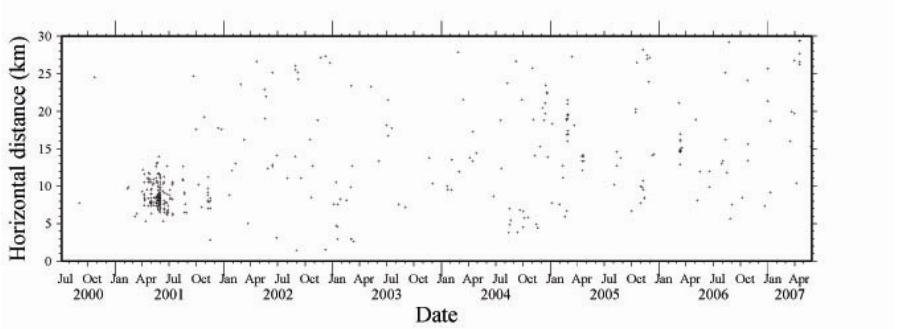

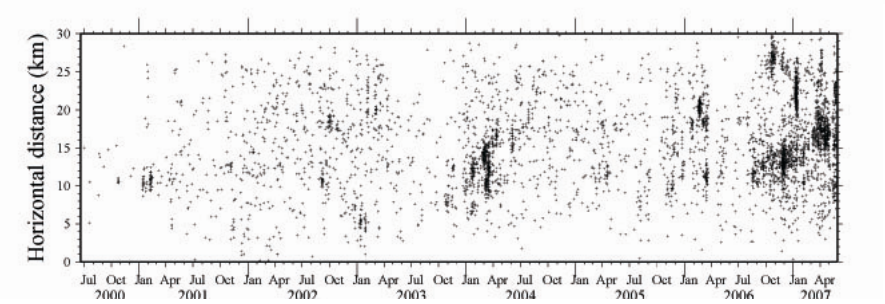

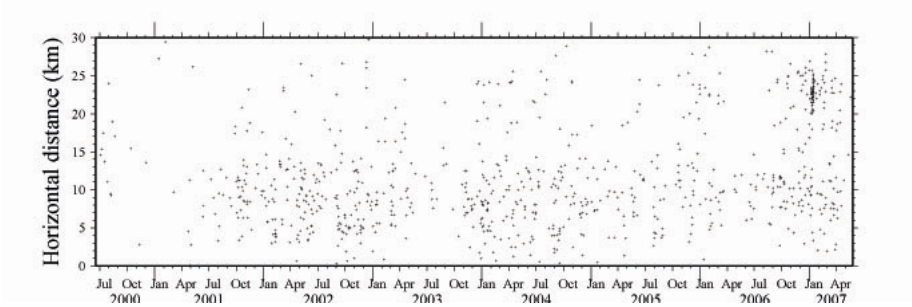

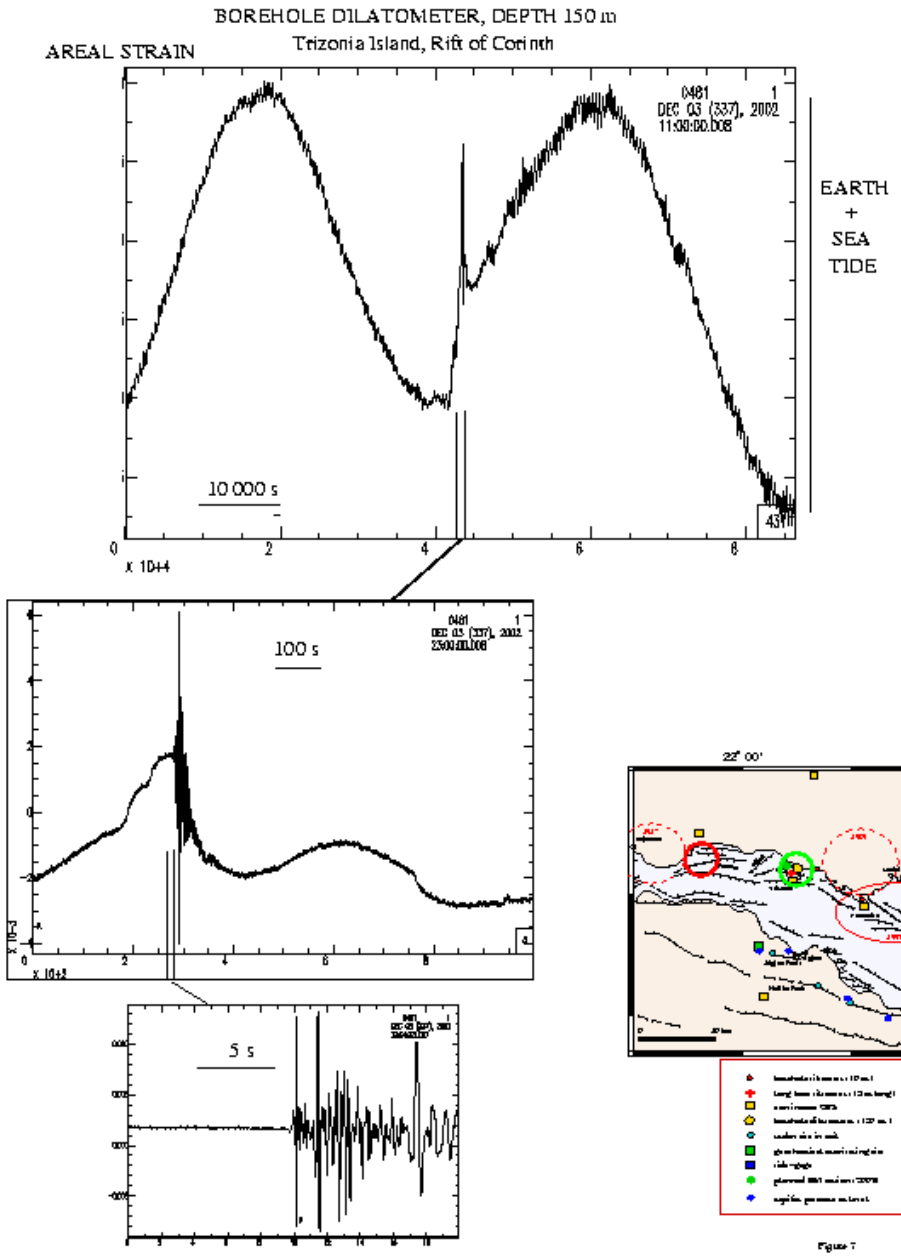

Slow deformation monitoring on Trizonia Island

(Bernard and Boudin, 2004)

+ 5 Continuous GPS stations

Seismic activity for the 2000-2004 period

- Vertical cross section oriented N 15°E : The so called low dipping zone exhibits a complex structure with faults rooting down to 12-14 km

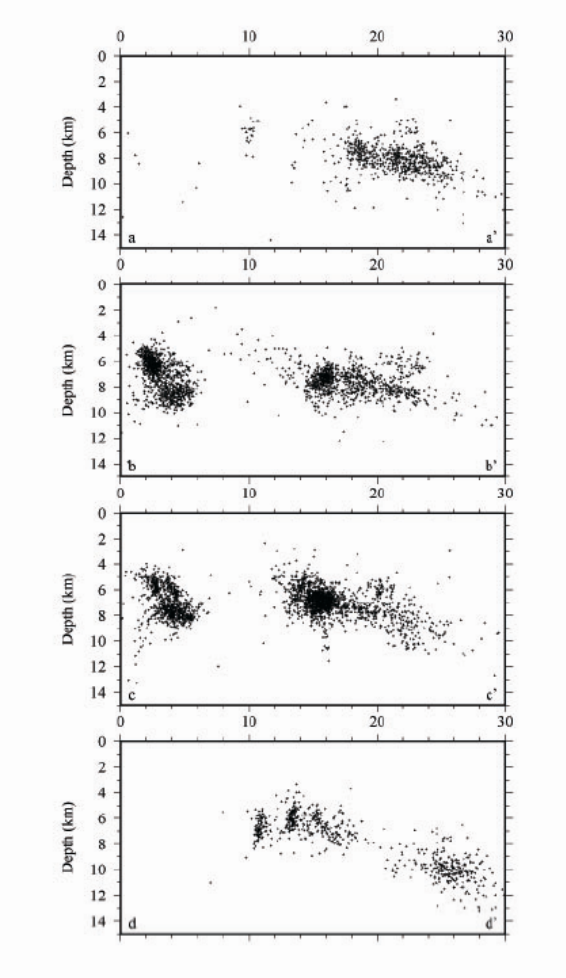

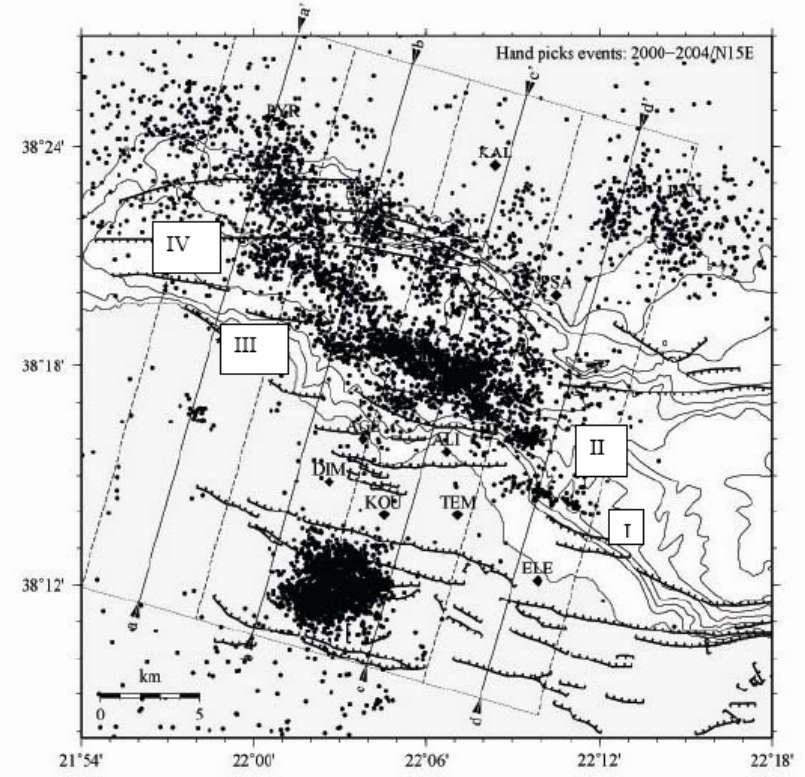

The Oct. 2003 – June 2004 swarm activity: Is there fluid diffusion ?

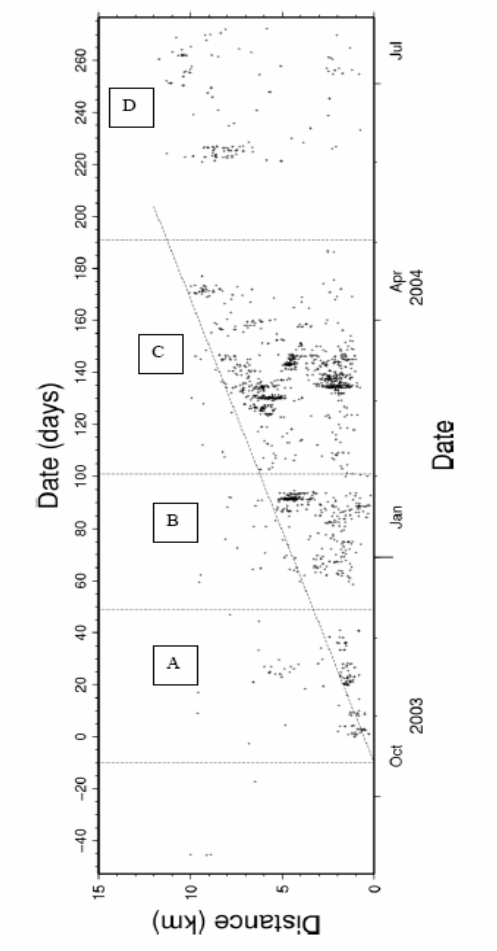

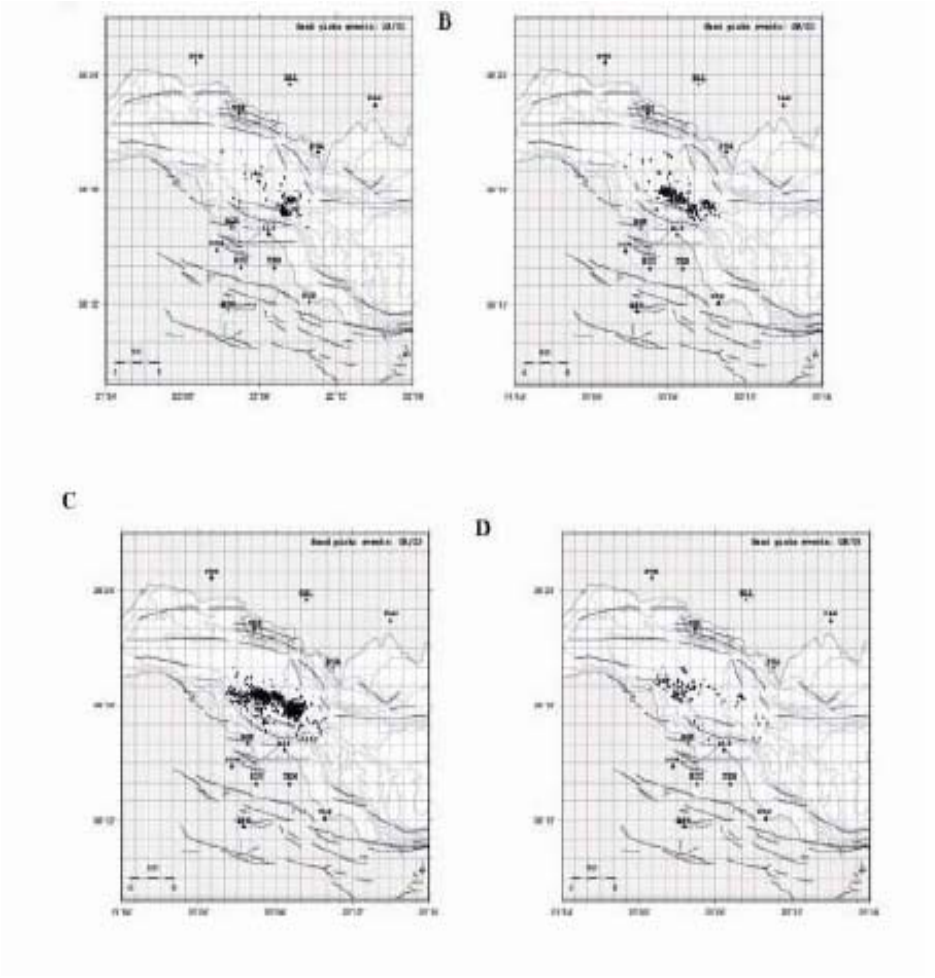

2003-2004 Swarm: event depth migration

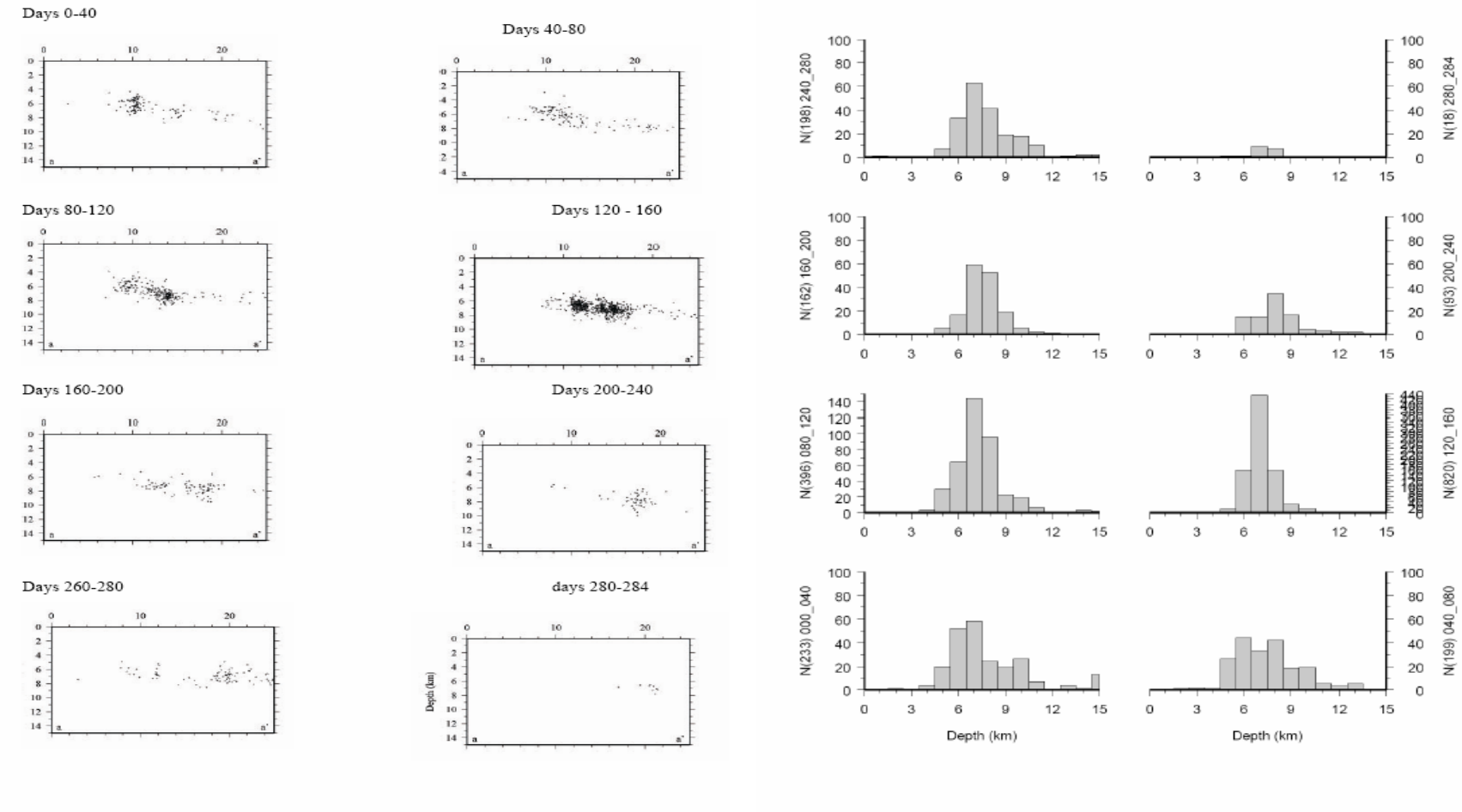

Simplified cross section for ICDP supported AIG10 well

(Cornet et al., Naville et al., Rettenmayer et al., CR-Geosciences, 2004)

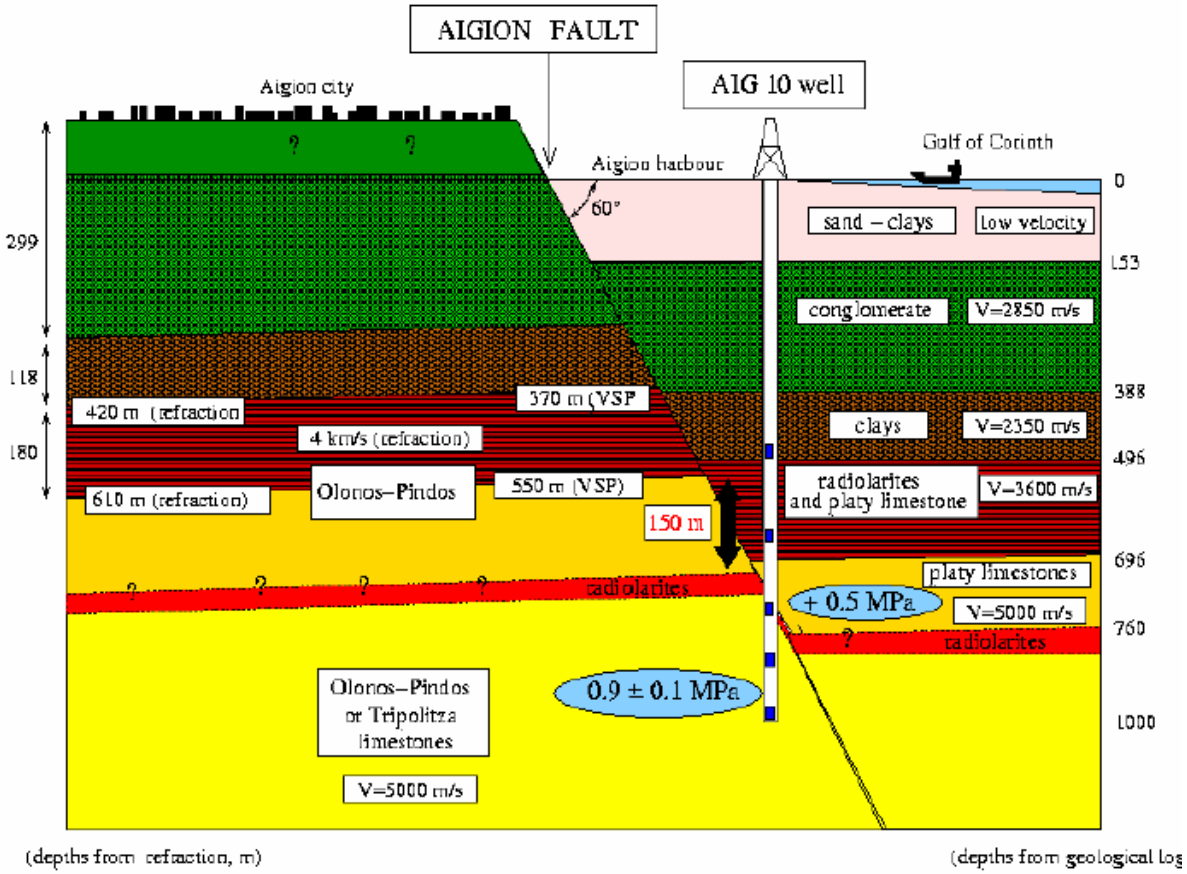

- Fault length : between 10 and 15 km
- Age of the fault of the order of 100 ky
- Mean fault velocity from 1.6 to 4.3 mm/y (according to paleosismology by trenching)

The cataclastic zone and the clay fault core

On the hydraulic properties of faults

from Nojima fault – Locker et al. (2000?)

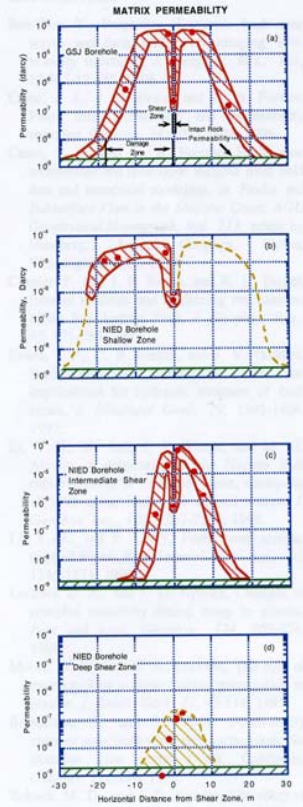

Figure 4. Profiles of matrix permeability measured at 50 MPa effective confining pressure. The three upper fault crossings show a low permeability shear zone axis surrounded by high permeability damage zones. The deep shear zone is partially sealed and was apparently not activated by the Kobe earthquake.

- Faults constitute hydraulic barrier perpendicularly to the fault direction but are hydraulically conductive parallel o the fault direction

Geophysical logs and hydraulic characterization (Gurgia et al, 2004; Daniel 2004)

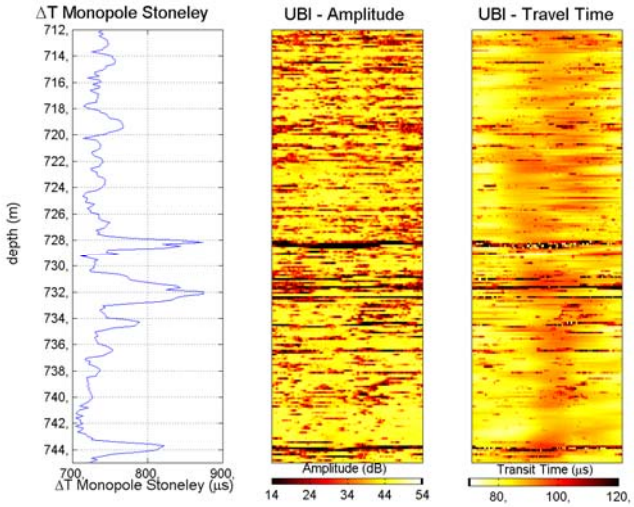

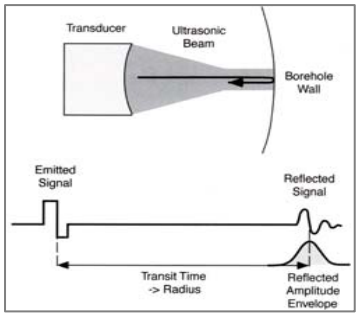

Left : platy limstone above h fault

Down : karst in limestone from the gavrovo Tripoliza Nappe

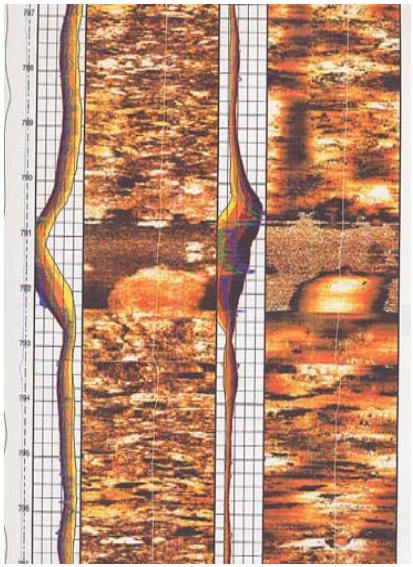

- Test at 200 m :
  Hydraulic conductivity 2.7 10^{-5} ms^{-1}, brackish water, 18 ° C
- Test at 735 m :
  40 l/min production; overpressure equals 0.5 MPa
  Hydraulic conductivity10^{-7} m/s; fresh water (less than 1g/l),
- Production test open-hole 710 - 1000 m, conducted at the end of drilling (sept. 2002) :
  1 MPa overpressure; Production flow rate 48 m^3/h during 3 d, 32 °C, fresh water
- Production observed sept. 2003
  250 m^3/h, heavy in sulfur, no tritium; age > 60 y;

Stress field in the vicinity of the Fault

(Sulem, 2007; Prioul et al. 2004)

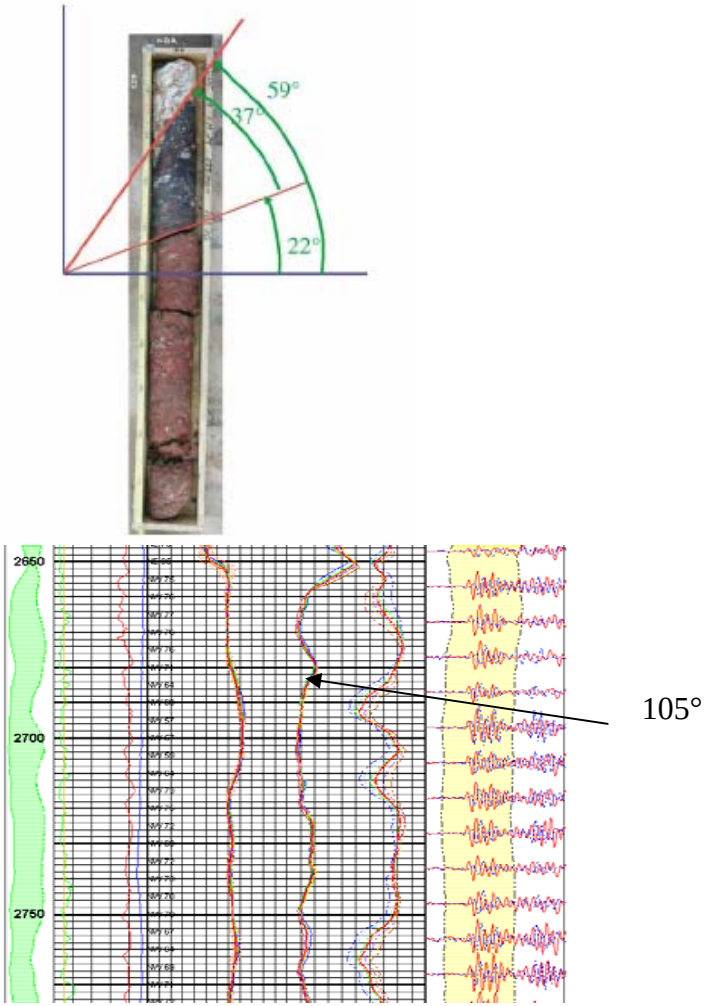

- From the laboratory characterization of the mechanical properties of the fault clay core (in particular « contractancy » during plastic deformation), maximum principal stress component found to be perpendicular to mean fault plane
- Anisotropy as determined from dipole sonic log, shows intermediate principal stress is parallel to fault direction (N 110°E)

Temperature and water pressure in AIG10

(Doan et Cornet, EPSL, 2007a; GRL, 2007b)

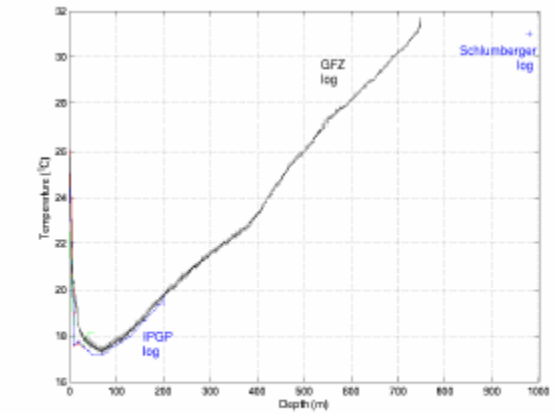

FIG. 1 – Profils thermiques établis par l'IPGP et par GFZ

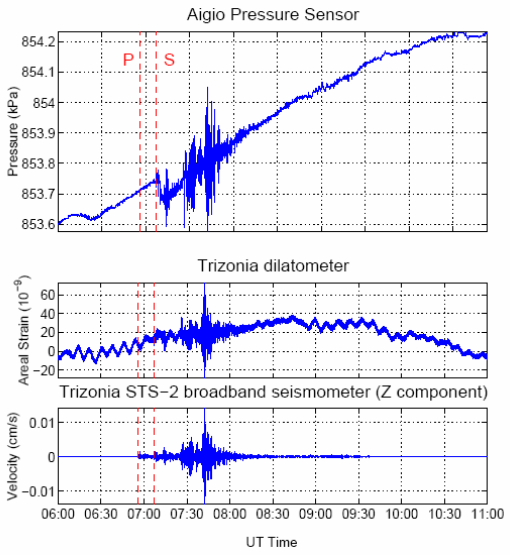

- Heat flow : 53 mw/m^2; convection in the karst
- Pressure gauge sensitivity : 10^{-4} μstrain
- Karst storativity : 7.7±2 10^{-7} m^{-1}
- Karst permeability :~ 10^{-12} m^2
- Upper and lower aquifers are confined

- Some teleseisms induce local effects

Downhole Instrumentation deployed June 17 2007

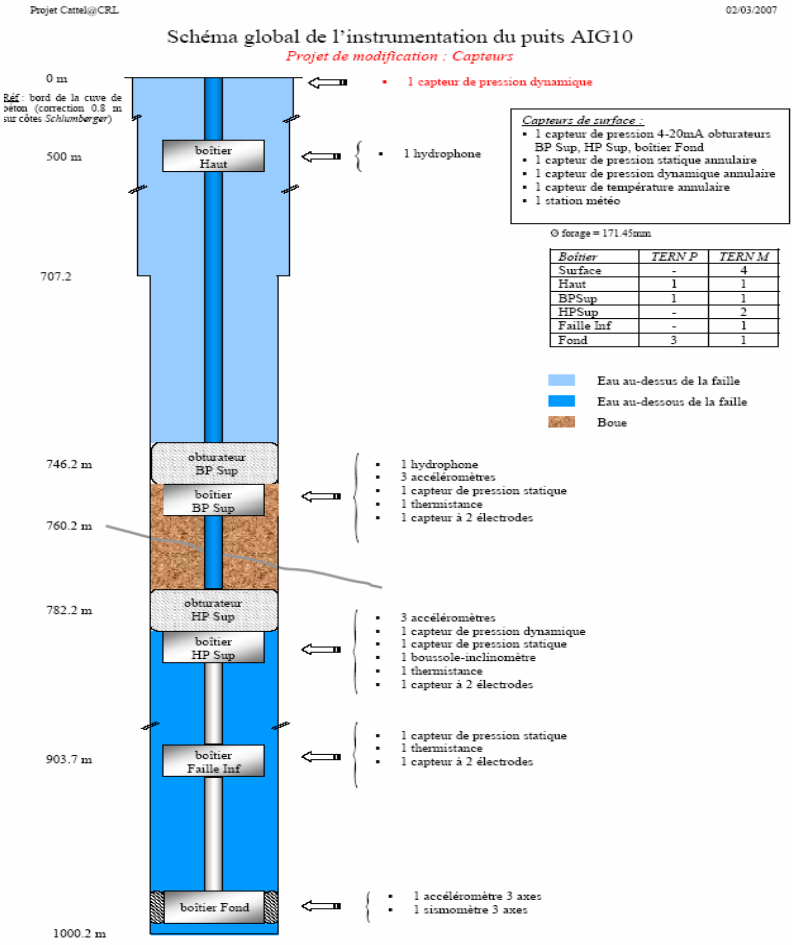

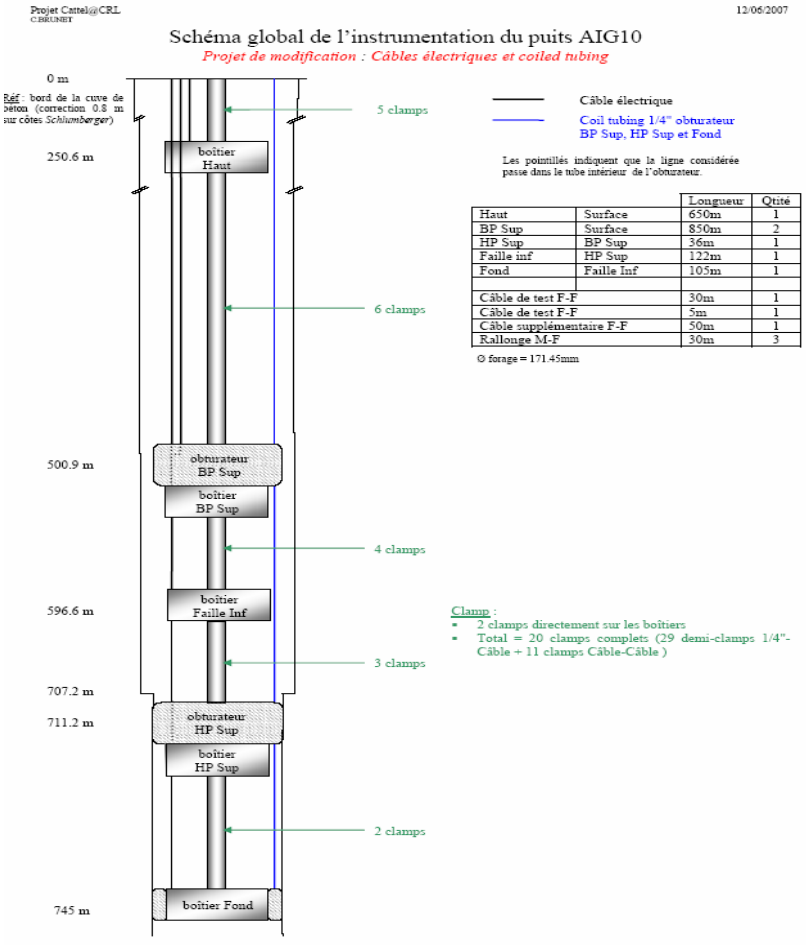

First results from the downhole pressure recording

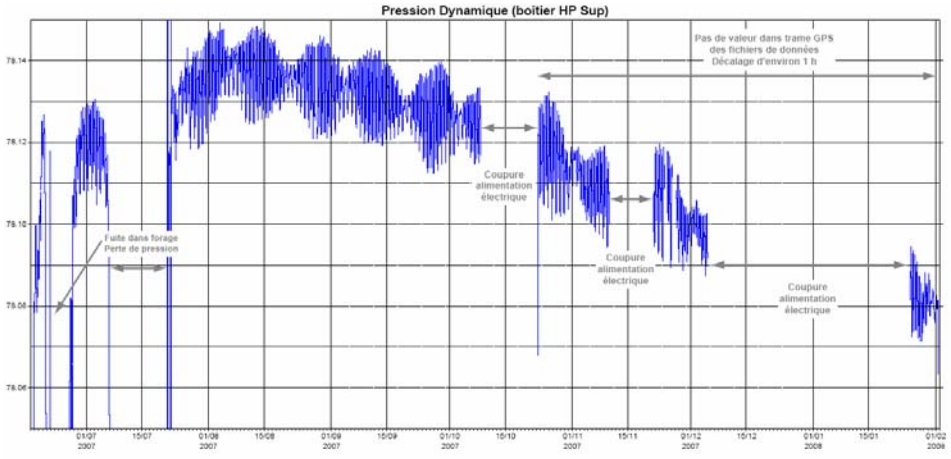

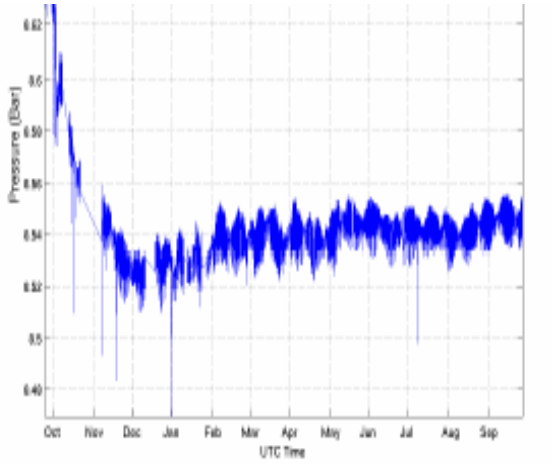

- Top : June 2007-Feb 2008,
  production flow rate 11 m^3/h
- Right : Oct. 2003-sept. 2004
  Production flow rate 250 m^3/h (sept. 2003)

Examples of seismic signals

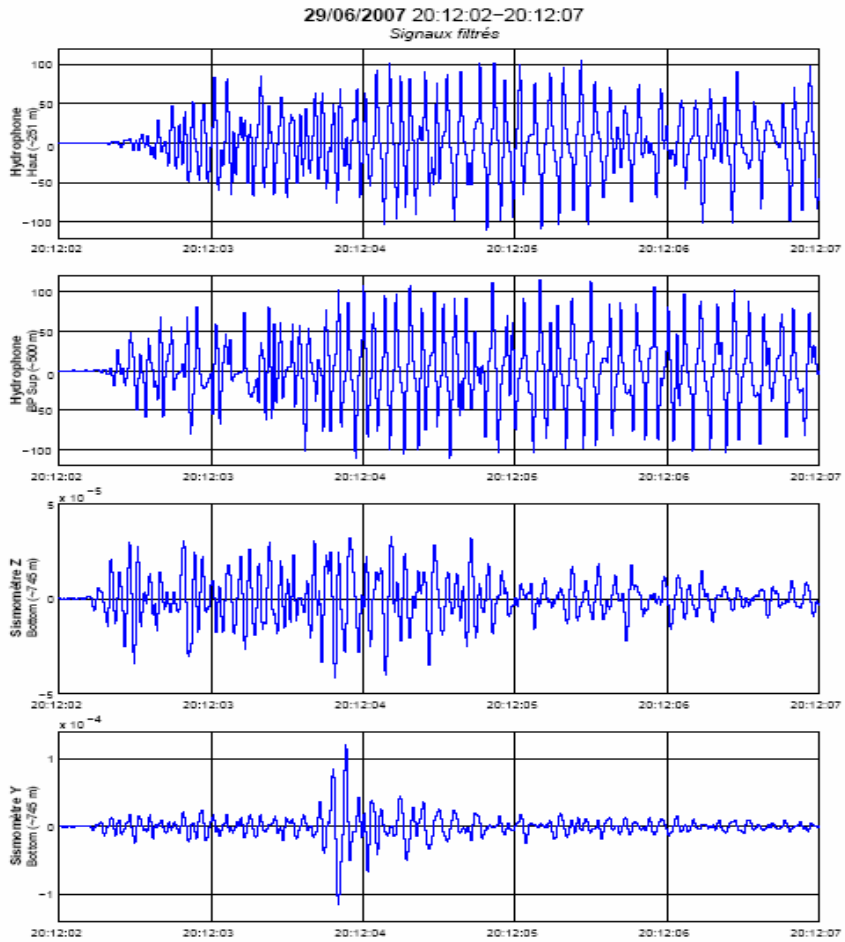

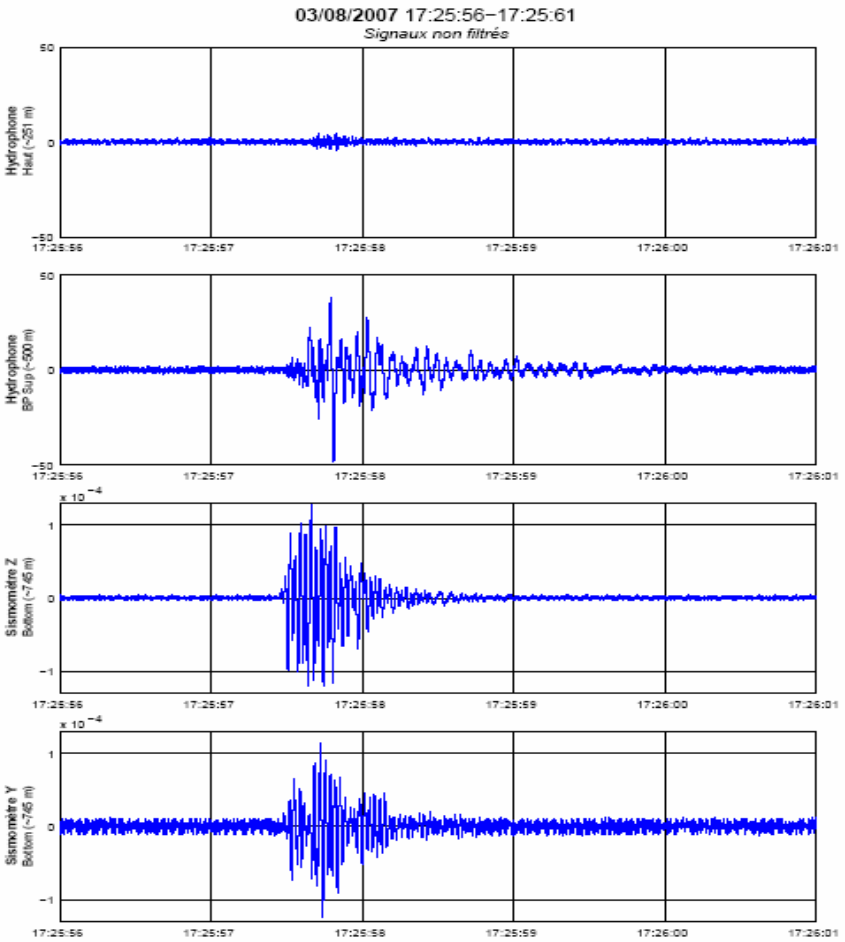

Example of seismic signal and statistics

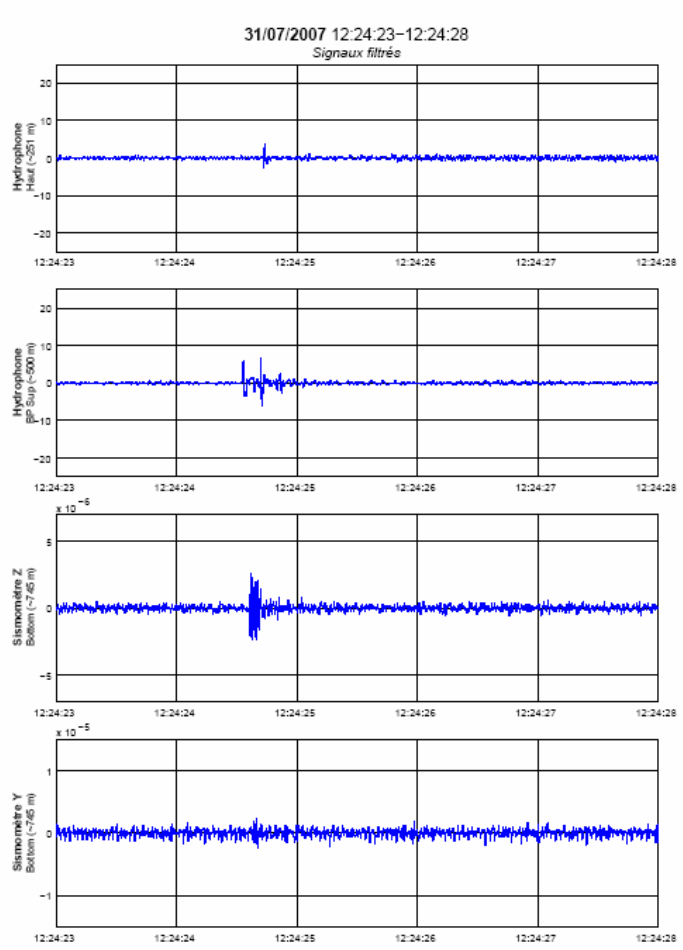

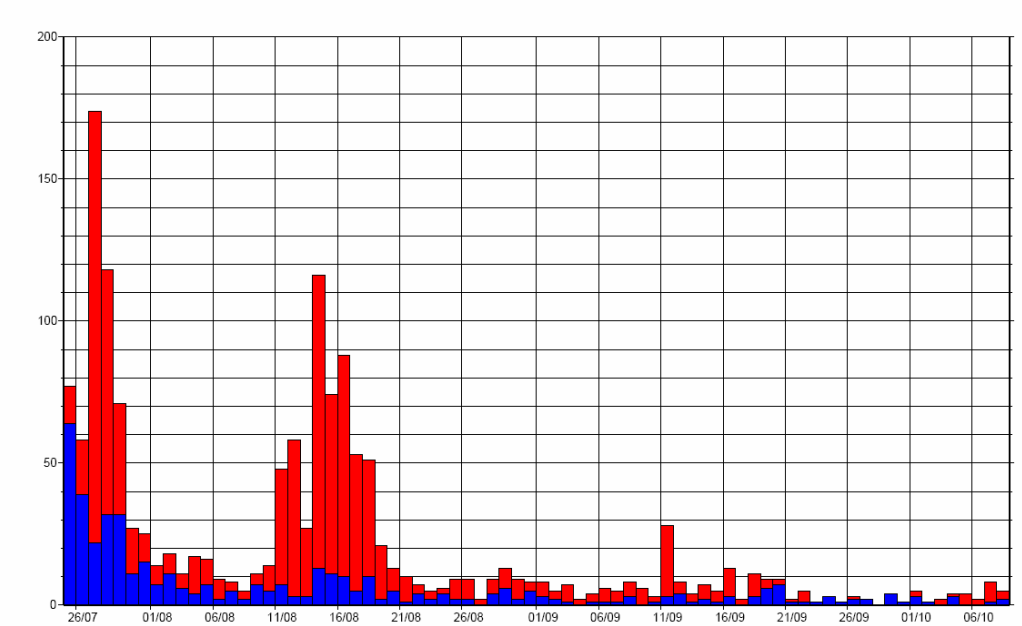

Migration direction during the 2001 and 2006-2007 swarms

- 2006-2007

Days 0-80

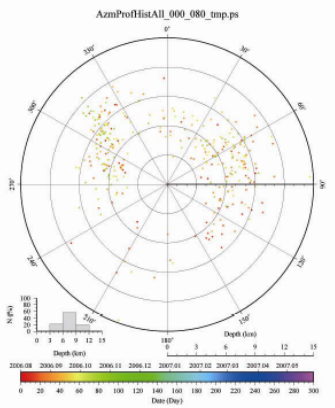

Days 80-180

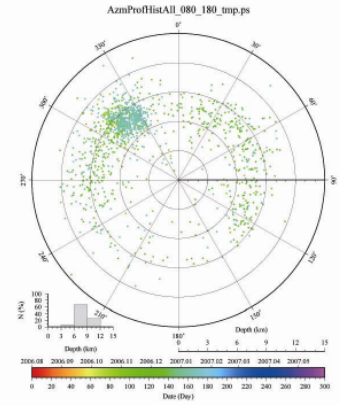

Days 180-300

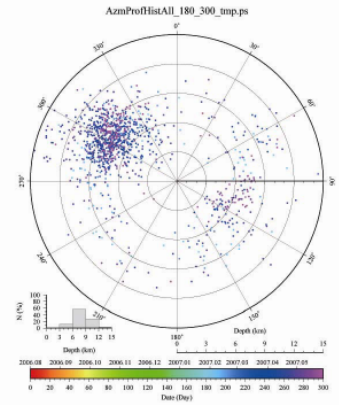

- 2001

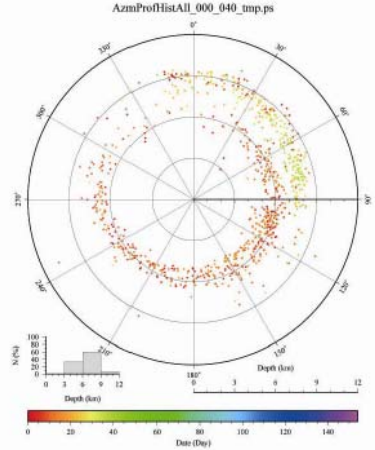

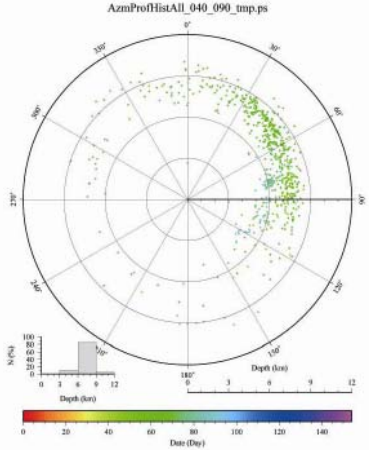

Calcite cements in fault material and water geochemistry:

upward growth of faults, with alternation of seismic and aseismic growth, without mantellic fluids percolation (Géraud et al., Tectonophysics, 2007)

- Aigion (AIG10) and Pyrgaki faults; analysis of carbon and oxygen isotopic composition yields information on fluid origins (deep crustal, marine, meteoric; after EOST-CGS)

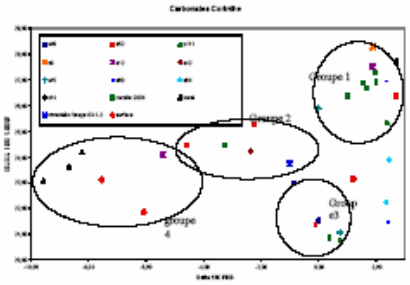

Figure 7.- Composition isotopique des ciments de calcite

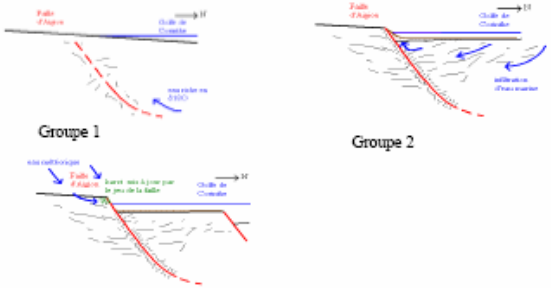

Figure 8.- model de circulation

- Analysis of calcite deposits in fault gouge (UMR5559 et 5573) :detection of seismic and aseismic deformation by Cathodoluminescence

- Helium isotopic analysis in both natural springs and cements in fault gauge (B. Marty, CRPG-Nancy); no fluids of mantellic origin

Illite Crystallinity index for defining crystallization temperature: preliminary results (Y. Géraud, EOST)

A set of 40 samples is analysed coming from faults and fractures of the AIG-10 borehole. They are filled by a mix of clays, quartz and calcite

Illite Rx diff signature

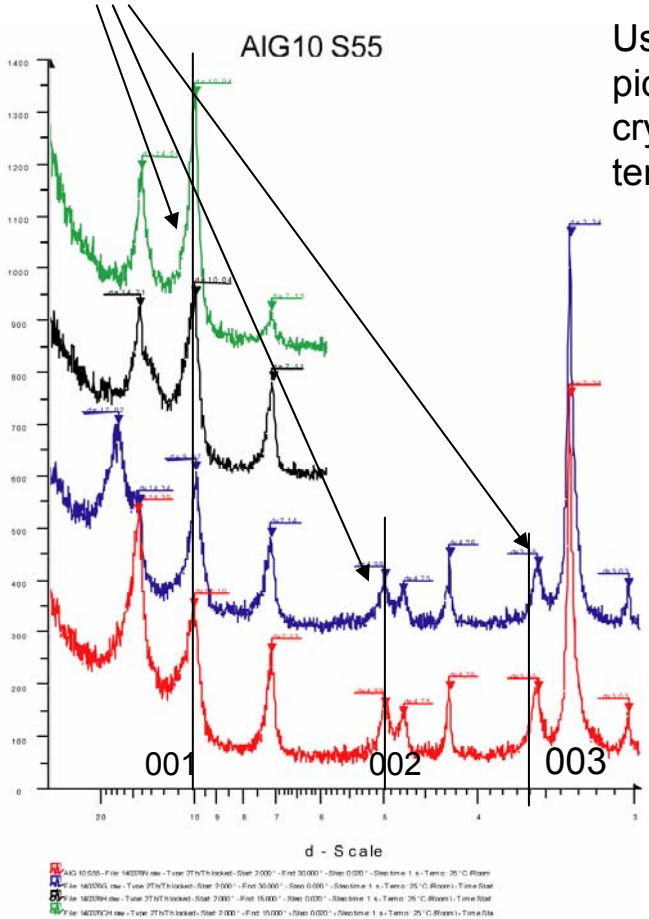

Use of MacDiff to define the shape and the width (for half heigth) of each pick, this last parameter is an indicator of the crystallinity (IC, for illite crytallinity). The cross-plot of IC picks (001, 002) gives the crystalisation temperature using Kübler's data (Frey, 1988; Ferreiro Mählmann, 1994)

Domain of the AIG-10 samples, ranging from 200 and 70°C

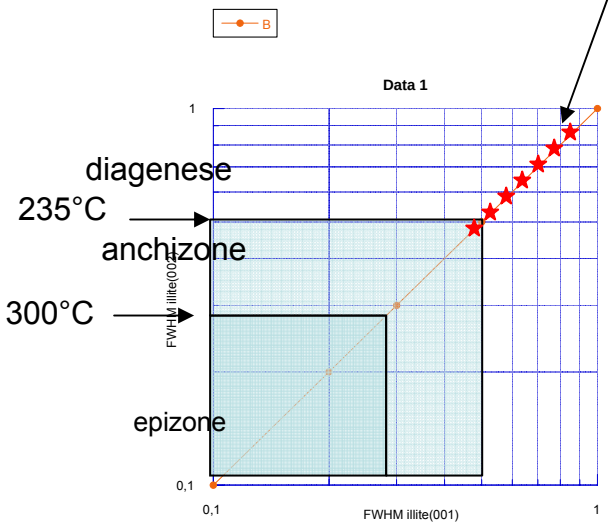

A first conclusion could be : A large set of fluid flowed in the fault and fracture network with a temperature ranging from 200 to 70°C

Conclusions from present work

- The Active Aigion fault is a hydraulic barrier in the direction perpendicular to the fault but exhibits a hydraulic diffusivity in the order of 10^4 cm^2/s, along the cataclastic zone, in th direction parallel to the fault

- Because of the high Peloponnesus topography, the normal fault system results in deep meteoric water percolation (at least down to 8 km)

- But near Aigion, some occasional up-flow of fluids of deeper origin are observed

- Present objective is to fix existing instrumentation in AIG10 well and to maintain observation at least till the end of 2009. Goal is to better understand the slow deformation process and the hydro-mechanical coupling

What next at CRL?

- In the context of the Plate Observatory System under development in the context of the European Union (EPOS Research Infrastructure), better understand the Hellenic subduction and its consequences on the Corinth Rifting process (next 10 years) with particular attention to slow deformation processes and hydromechanical coupling

- Drill to 5 km, near Aigion
  - to investigate the migrating fluids that percolate through the seismogenic zone (geochemistry and flow conditions) ;
  - to monitor the high frequency seismic activity
  - To investigate in situ the hydromechanical behaviour of normal faults (objective 2011).